

# Environmental Controls on Observed Spatial Variability of Soil Pore Water Geochemistry in Small Headwater Catchments Underlain with Permafrost

Nathan Alec Conroy,<sup>1\*</sup> Jeffrey M. Heikoop,<sup>1</sup> Emma Lathrop,<sup>1,2</sup> Dea Musa,<sup>1</sup> Brent D. Newman,<sup>1</sup> Chonggang Xu,<sup>1</sup> Rachael E. McCaully,<sup>3</sup> Carli A. Arendt,<sup>3</sup> Verity G. Salmon,<sup>4</sup> Amy Breen,<sup>5</sup> Vladimir Romanovsky,<sup>6</sup> Katrina E. Bennett,<sup>1</sup> Cathy J. Wilson,<sup>1</sup> and Stan D. Wullschlegel<sup>4</sup>

<sup>1</sup>Earth and Environmental Sciences Division, Los Alamos National Laboratory, Bikini Atoll Road, Los Alamos, New Mexico, 87545, [USA](#)

<sup>2</sup>Center for Ecosystem Science and Society, Department of Biological Sciences, Northern Arizona University, Flagstaff, AZ, 86011, USA

<sup>3</sup>Department of Marine Earth and Atmospheric Sciences, North Carolina State University, Raleigh, North Carolina, 27695, [USA](#)

<sup>4</sup>Biological and Environmental Systems Science Division and Climate Change Science Institute, Oak Ridge National Laboratory, Oak Ridge, Tennessee, 37831, [USA](#)

<sup>5</sup>International Arctic Research Center, P.O. Box 757340, University of Alaska, Fairbanks, Alaska 99775-7340, USA

<sup>6</sup>Geophysical Institute, University of Alaska Fairbanks, Fairbanks, Alaska, 99775, [USA](#)

Correspondence to: Nathan Alec Conroy (nconroy@lanl.gov)

**Abstract.** Soil pore water (SPW) chemistry can vary substantially across multiple scales in Arctic permafrost landscapes. The magnitude of these variations and their relationship to scale are critical considerations for understanding current controls on geochemical cycling and for predicting future changes. These aspects are especially important for Arctic change modelling where accurate representation of sub-grid variability may be necessary to predict watershed scale behaviours. Our research goal was to characterize intra- and inter-watershed soil water geochemical variations at two contrasting locations in the Seward Peninsula of Alaska, USA. We then attempt to establish which environmental factors were important for controlling concentrations of important pore water solutes in these systems. The SPW geochemistry of 18 locations spanning two small Arctic catchments were examined for spatial variability and its dominant environmental controls. The primary environmental controls considered were vegetation, soil moisture/redox condition, water/soil interactions and hydrologic transport, and mineral solubility. The sampling locations varied in terms of vegetation type and canopy height, presence or absence of near-surface permafrost, soil moisture, and hillslope position. Vegetation was found to have a significant impact on SPW  $\text{NO}_3\text{NO}_2^-$  concentrations, associated with the localized presence of nitrogen-fixing alders and mineralization and nitrification of leaf litter from tall willow shrubs. The elevated  $\text{NO}_3\text{NO}_2^-$  concentrations were however, frequently equiposed by increased microbial denitrification in regions with sufficient moisture to support it. Vegetation also had an observable impact on soil moisture sensitive constituents, but the effect was less significant. The redox conditions in both catchments were generally limited by Fe reduction, seemingly well-buffered by a cache of amorphous Fe hydroxides, with the most reducing conditions found at sampling locations with the highest soil moisture content. Non-redox-sensitive cations were affected by a wide variety of water-soil interactions that affect mineral solubility and transport. Identification of the dominant controls on current SPW hydrogeochemistry allows for qualitative prediction of future geochemical trends in small Arctic catchments that are likely to experience warming and permafrost thaw. As source

Formatted: Subscript

Formatted: Subscript

39 areas for geochemical fluxes to the broader Arctic hydrologic system, geochemical processes occurring in these  
40 environments are particularly important to understand and predict with regards to such environmental changes.

## 41 **1. Introduction**

42 Permafrost thaw in the Arctic is causing significant changes to landscape structure (Kokelj and Jorgenson, 2013;  
43 Rowland et al., 2010), hydrology (Hiyama et al., 2021; Kurylyk et al., 2021; Liljedahl et al., 2016; Vonk, Tank, and  
44 Walvoord, 2019; Walvoord and Kurylyk, 2016), vegetation (Lara ~~et al., Nitzte, Grosse, and McGuire~~, 2018; Myers-  
45 Smith et al., 2011; Sturm, Racine, and Tape, 2001; K. D. Tape ~~et al., Hallinger, Welker, and Ruess~~, 2012; ~~K-~~Tape,  
46 Sturm, and Racine, 2006;), and biogeochemistry (O'Donnell et al., 2021; Frey and McClelland, 2009; Salmon et al.,  
47 2019; Vonk, Tank, and Walvoord, 2019). The integrated hydrogeochemical effects of these environmental changes  
48 are already apparent in the chemistry of the large Arctic rivers, where fluxes of carbon and nutrients are increasing,  
49 leading to enhanced nutrient loadings, with strong implications for the global carbon cycle (Bring et al., 2016; Fuchs  
50 et al., 2020; McClelland et al., 2016). While the watershed areas of large Arctic rivers are vast, recent studies suggest  
51 that solute concentrations in these large rivers are likely controlled by solute generation processes occurring at much  
52 smaller scales (Harms and Ludwig, 2016; Koch ~~et al., Runkel, Striegl, and McKnight~~, 2013; Shogren et al., 2019;  
53 Vonk et al., 2015).

54 While there is a rapidly growing body of literature focused on observing and understanding environmental changes  
55 over time with further Arctic warming, relatively few studies directly address the existing spatial variability, within  
56 catchments or across catchments, and we are not aware of any studies that have combined field observations with  
57 thermodynamic modelling in an effort to understand the causes of the existing spatial variability. Therefore, we have  
58 a limited understanding of the key environmental controls on the spatial distribution of soil pore water solute  
59 concentrations. In this study, we quantitatively evaluate the spatial variability of soil pore water (SPW) geochemistry  
60 within and between two distinct catchments underlain with permafrost, and then seek to identify the source of the  
61 observed spatial variability.

62 This study takes advantage of a scientifically diverse array of observations and datasets made available by the Next  
63 Generation Ecosystem Experiment (NGEE) Arctic project, sponsored by the US Department of Energy Office of  
64 Science. Most of the locations studied herein were selected by the NGEE Arctic project to provide co-located  
65 measurements in a wide range of vegetation types, nested within representative hillslopes and catchments. Although  
66 selected largely to represent a range of vegetation structure, such as shrub abundance and canopy height, these  
67 locations also have considerable variability in other environmental parameters including, but not limited to: soil  
68 moisture and temperature, presence or absence of near-surface permafrost, and maximum observed thaw depth (**Table**  
69 **1** and **Table 2**). The vegetation-delineated sampling approach ~~presented here~~ provides an opportunity to not only  
70 quantify the biogeochemical variability of SPW in Arctic environments, but also to investigate the root causes of that  
71 observed variability. Data from additional sampling locations, available from a ~~collaborative-co-located~~ study, were  
72 also utilized when possible.

73 Our overarching hypothesis is that vegetation-type and hillslope position are the dominant controls on spatial  
74 variability of SPW geochemistry ~~at the NGEE Arctic field sites located on the Seward Peninsula~~. Vegetation-type

75 seems likely to have a significant effect on SPW geochemistry both directly and indirectly. Indirect effects would  
76 include vegetation canopy impacts on soil moisture (through evapotranspiration and snow trapping). Direct effects of  
77 vegetation would include nutrient cycle changes resulting from the annual deposition of plant litter. Such a direct  
78 effect can be augmented at sites populated by alder shrubs due to this genus of deciduous shrubs ability to form a  
79 symbiotic relationship with nitrogen-fixing *Frankia*, which they host in underground root nodules. Nitrogen fixation  
80 associated with alders has previously been shown to accelerate local nitrogen cycling (Binkley et al., 1992; Clein and  
81 Schimel, 1995; Bühlmann et al., 2014). Directly, through the increased cycling of some solutes (e.g. increased nitrogen  
82 concentrations in the vicinity of alders, which add nitrogen to soils via a symbiotic relationship with nitrogen-fixing  
83 bacterium; Salmon et al., 2019), and indirectly, through effects on soil moisture (i.e. evapotranspiration and trapping  
84 of snow). Soil moisture will also affect SPW geochemistry, particularly of redox sensitive species, by limiting oxygen  
85 diffusion and thus controlling which regions develop anoxic/reducing geochemical conditions. Soil moisture impacts  
86 will likely be correlated with vegetation-type as well as hillslope position, and the presence or absence of perching  
87 layers, including permafrost, all of which impact the vertical and horizontal drainage characteristics of a watershed.  
88 Chemical species that are not redox-sensitive or controlled by biogeochemical reactions are likely to be  
89 ~~effeted~~affected by transport, solubility, and water/sediment/organic matter interactions, and therefore largely  
90 controlled by hillslope position as well as soil moisture.

91 Identifying the dominant controls on solute concentration variability within each catchment and across catchments  
92 will facilitate better projections of future soil pore hydrogeochemistry in permafrost landscapes, and how these  
93 signatures are related to changing soil moisture and increasing ~~in~~ tundra shrub abundance in a changing Arctic (Bring  
94 et al., 2016; Myers-Smith et al., 2011; Prowse ~~et al.~~, Bring, Mård, and Carmack, 2015; Salmon et al., 2019; Sturm et  
95 al., 2001; ~~K. D.~~ Tape et al., 2012; ~~K.~~ Tape et al., 2006; Wrona et al., 2016, 2016). Arctic warming and associated  
96 permafrost thaw will increase hydrological connectedness between terrestrial and aquatic environments through  
97 deepening of the active layer and the formation of deeper, more coherent groundwater flow paths (Bring et al., 2016;  
98 Harms and Jones, 2012; Prowse, ~~Bring, Mård, Carmack,~~ et al., 2015a; Prowse, ~~Bring, Mård, and Carmack,~~ et al.,  
99 2015b). Meanwhile, changes in hydrogeochemical signatures in larger Arctic rivers are likely to originate in smaller  
100 catchments (McClelland et al., 2016; Prowse ~~et al.~~, ~~Bring, Mård, and Carmack,~~ 2015; Shogren et al., 2019; Spence,  
101 ~~et al., Kokelj, McCluskie, and Hedstrom,~~ 2015). In this sense, changes in hydrogeochemistry in small Arctic  
102 catchments not only impact hydrogeochemistry at much larger scales, but also prognosticate the future  
103 hydrogeochemistry of larger Arctic rivers.

## 104 2. Methods

### 105 2.1 Site Descriptions

106 This study focuses on two sites with permafrost on the Seward Peninsula of western Alaska, the Teller-27 Catchment  
107 and the Kougarak-64 Hillslope (**Figure 1**). The Teller-27 Catchment, henceforth “Teller,” is a small (~2.25 km<sup>2</sup>)  
108 headwater catchment located west of mile marker 27 along the Nome-Teller Highway northwest of Nome, Alaska.  
109 The Kougarak-64 Hillslope, henceforth “Kougarak,” is a hillslope (~2.0 km<sup>2</sup>) located west of mile marker 64 along

Formatted: Font: Italic

Formatted: Font: Not Italic

Formatted: Superscript

Formatted: Superscript

110 the Nome-Taylor Highway northeast of Nome, Alaska. We utilized data from “intensive stations” at both Teller and  
111 Kougarak where concentrated, multi-year, co-located observations of soil water chemistry, vegetation characteristics,  
112 soil moisture and temperature, and other measurements have been collected as part of the NGEE Arctic Research  
113 Project. These are identified as TL# (Teller Station #) or KG# (Kougarak Station #) in **Figure 2** and **Figure 3**,  
114 respectively. It should be noted that Teller and Kougarak are not “paired watersheds” in the classical sense, differing  
115 in only one major characteristic, which provides the basis for comparison. Instead, Teller and Kougarak differ in many  
116 respects and are both representative of the broad range of hillslope conditions common on the Seward Peninsula.  
117 Detailed descriptions of Teller and Kougarak have been published previously (Jafarov et al., 2018; Léger et al., 2019;  
118 Philben et al., 2019, 2020; Salmon et al., 2019; Yang et al., 2020), therefore, only the catchment characteristics that  
119 are probable sources of variability in SPW chemistry will be highlighted here.

120 Teller is a discrete catchment with a well-defined central drainage, a vertical declivity of approximately 200 m, and a  
121 catchment area of approximately 2.25 km<sup>2</sup>. Temperature probes, soil pits, coring activities, and geophysical  
122 interpretations at Teller have confirmed the catchment is underlain with discontinuous permafrost (Léger et al., 2019).  
123 The upper shoulder of Teller (near Station 5, **Figure 2** and **Figure 5**) is underlain with near-surface permafrost and  
124 appears to be a degraded peat plateau. The resultant microtopography of the degraded peat and the shallow perching  
125 horizon caused by the permafrost creates a landscape of unsaturated peat mounds surrounded by ponds and saturated  
126 soils. Downslope of the peat plateau, the Teller hillslope has highly variable soil moisture and vegetation (**Table 1**).  
127 The microtopography within the lower footslope looks similar to the upper shoulder, but the peat appears more  
128 severely degraded and the cause of the perched water table is less clear. Léger et al. (2019) suggest the presence of  
129 permafrost at a depth of 1 – 2 m at Teller Station 9 (**Figure 2**), but the perching could also be caused by a layer of silt,  
130 at a depth of approximately 30 cm (Graham et al., 2018). The full extent of permafrost and silt in this region of the  
131 catchment remains unknown, but the thaw depth in July 2018 was greater than 1 m and maintained a perched water  
132 table (Philben et al., 2020), suggesting perching could be the result of silt rather than permafrost. Vegetation type,  
133 moisture content, permafrost extent, and hillslope position for all Teller Stations are summarized in **Table 1**.

134 Kougarak differs in many ways from Teller, although both have characteristics that are typical of hillslopes on the  
135 Seward Peninsula. Kougarak is a convex hillslope, with a vertical declivity of approximately 70 meters. The study  
136 area at Kougarak is approximately 2.0 km<sup>2</sup>. Soil temperature measurements at Kougarak suggest that the vast majority  
137 of the site is underlain by shallow continuous permafrost (Romanovsky, Cable, and Dolgikh, 2020a); Kougarak  
138 Station 5 is an exception, where the permafrost is deeper (Romanovsky et al., 2020a). The upper shoulder of Kougarak  
139 is a well-drained rocky outcrop composed of metagranitic rock (Hopkins et al., 1955; Till, Dumoulin, Werdon, and  
140 Bleick, 2011). Saturated soils are not prevalent until the footslope and the lower backslope, where Kougarak Stations  
141 2, 11, 10, 1, and 6 are situated (**Figure 3**). The lower backslope is characterized by persistent saturation between  
142 ubiquitous tussocks, formed by the tussock cotton grass *Eriophorum vaginatum*. The tussock-lichen tundra at  
143 Kougarak introduces microtopography and spatially variable saturation; in this sense, the Kougarak tussocks are  
144 analogous to the peat mounds and hummocks at Teller, but on different spatial scales and formed by different  
145 processes. Kougarak has numerous patches of alder shrubland in an altitudinal band within the upper backslope; it  
146 should be emphasized that Teller lacks tussock-lichen tundra and alder (*Alnus viridis* ssp. *fruticosa*) shrubs that are a

Formatted: Superscript

Formatted: Superscript

147 feature of Kougarak. While continuous permafrost largely remains, the Kougarak site appears to be undergoing  
148 environmental changes as evidenced by an increase in alder coverage over the past decades (Salmon et al., 2019). Soil  
149 profiles underneath the alder patches are rocky with shallow bedrock and warmer permafrost (**Table 2**). Shrub tundra  
150 (alder savanna in tussock tundra and willow-birch tundra) dominates the lower backslope, where the annual active  
151 layer thickness is typically less than 100 cm. Vegetation type, moisture content, permafrost extent, and hillslope  
152 position at all Kougarak stations are summarized in **Table 2**.

## 153 2.2 Sampling & Analytical Approach

154 SPWs were sampled using two complimentary techniques. Fiberglass wicks (Frisbee [et al.](#), [Phillips, Campbell, and](#)  
155 [Hendriekx](#), 2010) were deployed in the upper 30 cm of soils at stations where shallow soils were unsaturated. These  
156 wicks were left in place from year-to-year and only replaced if damage was observed or suspected. The sample  
157 reservoirs from the wicks were collected whenever possible, usually a few times each summer. MacroRhizons  
158 (Rhizosphere Research Products; Netherlands) were used at stations that were more saturated, also targeting the upper  
159 30 cm of soils. Both techniques were used at stations of intermediate saturation, where both could be deployed  
160 effectively. MacroRhizons represent a relatively discrete temporal sampling event (minutes to hours), whereas wicks  
161 represent a cumulative water collected over longer periods (weeks to months). It is in this sense, that the two techniques  
162 are complimentary. Unfortunately, due to saturation variability both techniques could not be used at all stations and  
163 conditions at some Kougarak stations were sometimes too dry to collect meaningful volumes of SPW using either  
164 method. Additional SPW data from Kougarak were supplemented from a separate study focused on alder-related  
165 nutrient dynamics (McCaully et al., [2022In-Review](#)). These data were collected by MacroRhizons and are captured  
166 as Kougarak Stations 10 – 13, which were not part of the original stations established by the NGEE Arctic Program.  
167 A total of 309 SPW samples from Kougarak were collected and analysed, whereas a total of 89 SPW samples from  
168 Teller were collected and analysed.

169 After collection, SPW cation concentrations were measured in triplicate by inductively coupled plasma optical  
170 emission spectroscopy (Optima 2100 DV; PerkinElmer, USA) following US EPA Method 200.7. Inorganic anion  
171 concentrations were measured by ion chromatography (DX-600; Dionex, USA) following US EPA Method 300.0. B,  
172 F, K, Na, and Si concentrations collected by wicks were excluded from the dataset due to known issues with these  
173 ions leeching from fiberglass wick samplers (Perdrial et al., 2014; Wallenberger and Bingham, 2009). This effect is  
174 illustrated in [Supplementary Figure 1](#) and the lack of such an effect for divalent cations is shown in [Supplementary](#)  
175 [Figure 2](#). Comparison of data from wicks and MacroRhizons, along with the observations from (Perdrial et al., 2014),  
176 demonstrates that remaining constituents discussed herein were not affected by collection with fiberglass wicks.  
177 Alkalinity, pH, and  $E_H$  are all critical geochemical parameters that are susceptible to change during storage (Petron  
178 [et al.](#), [Hinzman, Shibata, Jones, and Boone](#), 2007); because of the large amount of data from wicks these parameters  
179 were not considered further, except in the context of thermodynamic modelling.

180 Observations related to vegetation, soil moisture, and permafrost extend were compiled from datasets made available  
181 by the NGEE Arctic project and are given for Teller in **Table 1** and for Kougarak in **Table 2**. The reported soil  
182 moisture contents were derived from an average of gravimetric measurements (2017 and 2018) and time domain

Formatted: Font: Bold

Formatted: Font: Bold

183 reflectometry measurements (2017 and 2019), and from remotely-sensed P-band Synthetic Aperture Radar (2017).  
184 End-of-winter snow depths were measured in March and April of 2016, 2017, and 2018. The annual average ground  
185 temperature was measured using in-situ temperature sensors (HOBO U30 DataLogger) at a depth of 1.5 meters below  
186 the ground surface (Romanovsky et al., 2020a; Romanovsky, Cable, and Dolgikh, 2020b) and the active layer  
187 thicknesses were determined by frost probe in September 2019 at the end of the growing season. Vegetation data were  
188 collected at the peak of the growing season in mid to late July 2016 and 2017 at the NGEE Arctic Kougarok and Teller  
189 field sites, respectively. The distribution of plant communities in the Arctic is primarily controlled by landscape,  
190 topography, soil chemistry, soil moisture, and the plants that historically colonized an area (Raynolds et al., 2019).  
191 Soil available rooting depth, which can be limited by shallow depths to bedrock, permafrost, or the water table, can  
192 also restrict plant growth and survival of certain species by reducing access to water and nutrients. We surveyed the  
193 dominant plant communities along each hillslope, which varied in their shrub abundance, canopy height, and structure,  
194 to characterize the vegetation composition at the sites following the recommended protocol of Walker et al. (2016).  
195 Extensive field site details and vegetation sampling methods are more thoroughly described in previous studies  
196 (Salmon et al., 2019; Langford et al., 2019; Yang et al., 2020; Sulman et al., 2021; Yang et al. 2021).  
197 For this study, we provide summary statistics for vegetation plots associated with intensive stations. Vegetation  
198 composition plots within each intensive station were chosen subjectively in areas of homogeneous and representative  
199 vegetation varying in size from 1 to 25 m<sup>2</sup> depending on canopy structure and height. The surveyed plot area was 1 ×  
200 1 m for all plant communities except for the taller stature willow-birch tundra, mesic willow shrubland (2.5 × 2.5 m),  
201 and alder shrubland (5 × 5 m). For each plot, all plant species (vascular plants, lichens, and bryophytes) were recorded  
202 along with visual estimates of their percent cover. For plots with multiple canopies, field cover estimates were recorded  
203 as absolute cover, meaning that the total cover per plot can be >100%. We calculated relative cover values (adding to  
204 100%) from the field data and use these for all subsequent analyses.  
205 Plant species were further aggregated into nine plant functional types (PFTs), groupings of plant species that share  
206 similar growth forms and roles in ecosystem function (Wullschleger et al., 2014), based on growth patterns and plant  
207 traits. PFTs in this study include: (1) nonvascular mosses and lichens, (2) deciduous and evergreen shrubs of various  
208 height classes, including an alder PFT, (3) graminoids, and (4) forbs. Photos of representative PFTs from both sites  
209 are given in **Supplementary Figures 9-17**. Canopy height was estimated within each plot for each PFT as the average  
210 of 4 measurements, including a maximum canopy height. Active layer depth was measured at the end of the growing  
211 season for all plots in September 2018 using a frost probe. A temperature probe was used to determine if the resistive  
212 layer was permafrost (<0 °C) or rock (>2 °C). Thaw depth is an average of 4 measurements from the vegetation plot  
213 corners.

Formatted: Superscript

Formatted: Font: Bold

### 214 2.3 Statistical Analysis

215 Principal Components Analysis (PCA) and the Mann-Whitney U-Test (MWUT) were both used to investigate  
216 dominant environmental controls on solute concentrations in SPWs at Teller and Kougarok. PCA is an exploratory  
217 data analysis tool that reduces the dimensionality of large complex datasets and considers how components (i.e. solute  
218 concentrations) vary together. Because PCA was predominately used as a screening tool to reveal geochemical

219 correlations that may not have been evident by traditional geochemical causations or inference, a detailed discussion  
220 of the PCA results is reserved to the Supplementary Materials. The MWUT was used to test for significant differences  
221 in solute concentrations between Teller and Kougarok (inter-site variability) and between stations at each site (intra-  
222 site variability). The MWUT is a non-parametric method of challenging a null hypothesis, which in this case is the  
223 assumption that the concentrations of a given solute are not systematically greater at either site nor at any particular  
224 station. Water chemistry data are typically not normally distributed and thus, non-parametric difference tests such as  
225 the MWUT are preferred. The MWUT challenges the distribution of values, not the means. In this work, the level of  
226 significance associated with the null hypothesis was operationally defined as 0.05, which equates to a 95 % chance  
227 that an observed statistical difference is real and not coincidental. This error rate is operationally defined per contrast  
228 (i.e. a 95 % chance that the observed statistical difference in nitrate concentrations between Teller Station 9 and Teller  
229 Station 7 is real or that the observed statistical difference in sulphate concentrations between Teller and Kougarok is  
230 real) as opposed to familywise (i.e. a 95 % chance that all of the observed/reported statistical differences are real and  
231 not coincidental). MWUTs were completed using the methods described in Corder and Foreman (2009) and PCA was  
232 completed using packages available in R statistical software, version 3.3.6 (Corder and Foreman, 2009; R Core Team,  
233 2020). For all analyses, concentrations below the method detection limit were operationally defined as half the  
234 detection limit, in agreeance with (Helsel, 2005, p. 43). While the emphasis of this study was on site/station (i.e.  
235 spatial) variability, it should be recognized that seasonal and inter-annual variability could also be significant. To  
236 minimize seasonal forcing on the variability observed, all SPW geochemical data presented were collected during the  
237 thaw season between June and September.

#### 238 **2.4 Thermodynamic Modelling**

239 To investigate thermodynamic controls on solute behaviour, particularly solubility limitations, thermodynamic  
240 modelling exercises were undertaken using PHREEQC, a thermodynamic geochemical modelling code, and  
241 PhreePlot, which facilitates repetitive PHREEQC calculations through looping (Kinniburgh and Cooper, 2011;  
242 Parkhurst and Appelo, 2013). Because this study was focused on elucidating the primary geochemical controls on  
243 solute concentrations in SPWs and not on developing a rigorous transport model, representative concentrations were  
244 used instead of station specific concentrations. Representative “low”, “median”, and “high” concentration conditions  
245 were proxied from the 25th, 50th, and 100th concentration percentiles, respectively, taken from both Teller and  
246 Kougarok (Supplementary **Table 4**). Meanwhile, representative pH and  $E_H$  ranges were determined either through  
247 direct measurement (pH), or indirectly by correlating dissolved  $Fe^{2+}$  concentrations and pH with a redox condition  
248 through geochemical models and the Nernst equation. Modelling exercises were performed at 25 °C—utilizing the  
249 phreeqc.dat database, with the only modification being the suppression of methane production by inorganic carbonate  
250 reduction. Modelling exercises were performed at the default PHREEQC modelling temperature (25 °C), as the  
251 selection of an alternative defensible temperature was non-trivial: temperatures on the Seward Peninsula span a very  
252 wide range and its unclear what temperature would be most suitable for mineral solubility limitation modelling.  
253 Ultimately, because the thermodynamic models were used as a tool understand what could be controlling soil pore  
254 water solute concentrations and were not intended to model the system or to predict future concentrations, the default

255 temperature was decided to be the most suitable. While there is some temperature dependence of mineral solubility,  
256 the differences in predicted solubility between 4 °C and 25 °C did not impact the interpretation of our results  
257 (Supplementary Figure 8). Methane production was “turned-off” to maintain carbonate availability under reducing  
258 conditions to help identify any possible carbonate minerals that could be precipitating. Because alkalinity was only  
259 measured in a small number of samples, carbonate concentration percentiles were estimated from charge imbalances.  
260 Alkalinity and charge imbalance were very well correlated in samples where alkalinity was measured  
261 (Supplementary Figure 3). Although not a particularly rigorous modelling exercise, this approach was sufficient to  
262 identify mineral phases that could be controlling solute generation processes through solubility limitations.

Formatted: Font: Bold

Formatted: Font: Bold

### 263 3. Results

#### 264 3.1 Physical Characteristics of Stations (Co-Located Studies)

265 Controls on the observed spatial variability of SWP solute concentrations at Teller and Kougarok stations were  
266 deduced, in part, from differences in physical features and conditions of each station. Quantitative measures of many  
267 of these physical characteristics were available from the interdisciplinary studies co-located at the Teller and Kougarok  
268 stations. The extent of permafrost, ground temperature, active layer depth, soil moisture content, snow depth,  
269 vegetation type, vegetation canopy height, dominant plant functional type, and hillslope position were all compiled  
270 from these co-located studies. Using these measures, the physical characteristics of each station are summarized in  
271 Table 1 and Table 2, grouped by vegetation type.

#### 272 3.1.2 Inter-site Variability: Teller versus Kougarok

273 Mann-Whitney U-Testing revealed that the concentrations of 14 of the 23 constituents analysed were significantly  
274 different ( $1.96 < |z|$ ) between Teller and Kougarok (Table 3). The effect size, a measure of how significantly different  
275 the concentrations were, were large for Na and F; medium-large for K and Si; medium for Al, Oxalate, B, Zn,  $\text{SO}_4\text{SO}_4^{2-}$   
276 , Fe, Ba, Ti, and  $\text{NO}_3^-$ ; and small-medium for Li. The terminology and thresholds for these semi-quantitative  
277 differences in correlation were taken from Corder and Foreman (2009). Mann-Whitney U-testing revealed that SPW  
278 concentrations of many constituents were significantly different between Teller and Kougarok (Table 3). When  
279 concentrations were significantly different between the sites, Kougarok generally exhibited the higher concentrations  
280 of the two. SPW concentrations of Na, F, K, Si, Al, oxalate, B, Zn, Fe, Ba, Ti,  $\text{NO}_2$ , and Li were all significantly  
281 greater at Kougarok than Teller, while only  $\text{SO}_4^{2-}$  concentrations were significantly greater at Teller. Meanwhile, the  
282 concentrations of Br,  $\text{NO}_3^-$ , Sr,  $\text{PO}_4$ , Mg, Cr, Mn, Cl, and Ca were not significantly different between Teller and  
283 Kougarok. When concentrations were significantly different between the sites, Kougarok generally exhibited the  
284 higher concentrations of the two. Only  $\text{SO}_4$  concentrations were significantly greater at Teller. The concentrations of  
285 Br,  $\text{NO}_3^-$ , Sr,  $\text{PO}_4$ , Mg, Cr, Mn, Cl and Ca were not significantly different between Teller and Kougarok. A summary  
286 of the inter-site MWUT results are given in Table 3 with the constituents that exhibited significant differences between  
287 the sites displayed over a darkened background.

Formatted: Subscript

Formatted: Superscript



288 **3.23 Intra-site Variability: Teller and Kougarok Stations**

289 Mann-Whitney U-Testing was also used to test for intra-site differences between stations at both Teller and Kougarok.  
290 Boxplots and compact letter displays are used to visualize the within-site variability of a select group of constituents  
291 of interest (COIs), which are given in **Figure 4**. Tables of the results of the intra-site MWUTs for all constituents that  
292 were monitored, including those that did not demonstrate some systematic inter-station variability or were not  
293 otherwise of interest, are given in the Supplementary Materials.

294 **3.3 Physical Characteristics of Stations (Co-Located Studies)**

295 Controls on the observed spatial variability of SPW solute concentrations at Teller and Kougarok stations were  
296 deduced, in part, from differences in physical features and conditions of each station. Quantitative measures of many  
297 of these physical characteristics were available from the interdisciplinary studies co-located at the Teller and Kougarok  
298 stations. The extent of permafrost, ground temperature, active layer depth, soil moisture content, snow depth,  
299 vegetation type, vegetation canopy height, dominant plant functional type, and hillslope position were all compiled  
300 from these co-located studies. Using these measures, the physical characteristics of each station are summarized in  
301 **Table 1** and **Table 2**, grouped by vegetation type.

302 **4. Discussion**

303 **4.1 Inter-site Variability: Teller versus Kougarok**

304 Mann-Whitney U testing revealed that SPW concentrations of many constituents were significantly different between  
305 Teller and Kougarok (**Table 3**). SPW concentrations of Na, F, K, Si, Al, oxalate, B, Zn, Fe, Ba, Ti, NO<sub>2</sub>, and Li were  
306 all significantly greater at Kougarok than Teller, while only SO<sub>4</sub> concentrations were significantly greater at Teller.  
307 Meanwhile, the concentrations of Br, NO<sub>3</sub>, Sr, PO<sub>4</sub>, Mg, Cr, Mn, Cl, and Ca were not significantly different between  
308 the two sites. Overall, the more frequent instance of significantly greater constituent concentrations at Kougarok  
309 suggests a systematic cause. The extensive low gradient toeslope (**Figure 2**) and lack of a well defined drainage  
310 channel at Kougarok, are likely causes of the systematically higher SPW solute concentrations at Kougarok. Water  
311 perching, the result of near surface permafrost in the lower backslope and toeslope, increases evapotranspiration and,  
312 thus, SPW solute concentrations. Meanwhile, the lack of a drainage channel at Kougarok suggests that runoff (and  
313 therefore solute exports) is more limited than at Teller. Without a relatively rapid export mechanism such as a stream  
314 channel, solute transport is likely limited to interflow within the Kougarok hillslope over much of the thaw season,  
315 allowing weathering products to increase to significantly greater concentrations than those observed at Teller, where  
316 a well defined drainage/export mechanism does exist. Field observations from pits at Kougarok confirm the present  
317 of interflow at the site. The exception to the general observation of elevated concentrations at Kougarok versus Teller  
318 was SO<sub>4</sub>. Although the cause of consistently higher SO<sub>4</sub> concentrations at Teller is unclear from the limited scope of  
319 this study, it seems likely to be due to a greater abundance of sulfidic bedrock material. The presence of sulfidic  
320 bedrock in the vicinity of Teller has been reported by mineral prospecting efforts (Brobst, Pinckney, and Sainsbury,  
321 1971; Herreid, 1966; Mulligan, 1965); we are unaware of any such reports near Kougarok.

## 4.2 Intra-site Variability: Teller and Kougarok Stations

Our interpretation of the major environmental controls on the observed spatial variability of SPW solute concentrations between stations are shown in Table 4. Each of these controls, including vegetation effects, soil moisture and redox effects, weathering, water/soil interactions and hydrological transport effects, and mineral solubility effects, is discussed-considered in detail in the following sections.

### 3.4.3.1 Vegetation Effects

Vegetation can influence hydrogeochemical variability directly via vegetation-induced changes to elemental cycling and soil moisture contents, or indirectly via the secondary impacts changes in soil moisture can have on mineral solubility or on the soil redox condition. The geochemical consequences of solubility and redox conditions are the focus of sections to follow, thus, this section will focus on direct vegetation effects via influences on elemental cycling and soil moisture via evapotranspiration and preferential trapping of snow.

$\text{NO}_3\text{NO}_2^-$  was the only COI that showed a distinct effect from vegetation via elemental cycling.- Elevated  $\text{NO}_3\text{NO}_2^-$  concentrations were associated with the presence of alder shrubs and, in some cases, willow shrubs.  $\text{NO}_3\text{NO}_2^-$  concentrations at both sites were generally low, with the exception of Kougarok Stations 3, 5, and 12, and Teller Station 7 (Figure 4). **Low to tall alder shrubs are the dominant vegetation type at Kougarok Stations 3 and 12 (Table 2).** Meanwhile, alders are present at Kougarok Station 5 despite the dominant vegetation type being low willow and birch shrubs. Kougarok Stations 3, 5, and 12 all have a significant alder presence. Alders increase soil nitrogen through a symbiotic relationship with nitrogen-fixing bacteria that reside in their root nodules, thus, an association between  $\text{NO}_3\text{NO}_2^-$  concentrations and alder vegetation is expected (Salmon et al., 2019).

Perhaps more noteworthy was ~~the elevated  $\text{NO}_2^-$  at Kougarok Station 5 and~~ the lack of elevated  $\text{NO}_3\text{NO}_2^-$  concentrations at Kougarok Stations 1, 2, 6, 10, and 11. The vegetation type at Kougarok Stations 1, 2, 6, 10, and 11 is alder savanna in tussock tundra, which is a mixed graminoid-shrub tundra with shorter stature and lower density of alder shrubs, yet nonetheless nitrogen input via alder derived nitrogen-fixation is anticipated to occur. The lack of elevated  $\text{NO}_3\text{NO}_2^-$  suggests either that 1) nitrogen-fixation in alder savanna in tussock tundra is insufficient to result in an increase in  $\text{NO}_3\text{NO}_2^-$  concentrations, 2) that the Kougarok footslope and lower backslope is very nitrogen-limited, and thus, that  $\text{NO}_3\text{NO}_2^-$  is largely consumed by vegetation as it is fixed, or 3) that microbes in the Kougarok footslope and lower backslope rapidly denitrify the available  $\text{NO}_3\text{NO}_2^-$  as a substitute for oxygen in their metabolisms. The smaller shrub size and density in the alder savanna in tussock tundra certainly results in less accumulated leaf litter relative to the denser and larger alder shrubland intensive stations, as such, it seems reasonable that less nitrogen would be available at stations in alder savanna in tussock tundra. Meanwhile, isotopic measurements of nitrogen downslope of alder patches at Kougarok Stations 12 and 3 also support the occurrence of denitrification (McCaully et al., In Review 2022). Therefore, we believe the lack of elevated  $\text{NO}_3\text{NO}_2^-$  concentrations at Kougarok Stations 1, 2, 6, 10, and 11 is a combination of less alder leaf litter and greater denitrification, than at Kougarok Stations 3, 5, or 12.

At Teller, only Station 7 exhibited elevated  $\text{NO}_3\text{NO}_2^-$  concentrations relative to the rest of the catchment (Figure 4). Teller Station 7 is dominated by tall willow shrubs and is relatively dry. Mineralization and nitrification of willow leaf litter coupled with limited microbial denitrification is the presumed cause of elevated  $\text{NO}_3\text{NO}_2^-$  concentrations at

Formatted: Heading 2,Sub\_Heading

Formatted: Subscript

Formatted: Subscript

Formatted: Subscript

Formatted: Font: Bold

Formatted: Not Superscript/ Subscript

Formatted: Not Superscript/ Subscript

Formatted: Superscript

358 Teller Station 7. Teller Station 2 also has tall willow shrubs but did not exhibit elevated  $\text{NO}_3\text{NO}_3^-$  concentrations.  
359 From the limited scope of this study, it is unclear why Teller Station 2 did not exhibit elevated  $\text{NO}_3\text{NO}_3^-$  while Station  
360 7 did, but we suspect that higher seasonal moisture content and greater microbial denitrification at Teller Station 2  
361 likely played a role. Also of note was that despite significant intra-site  $\text{NO}_3\text{NO}_3^-$  concentration differences, inter-site  
362 differences were not significant ( $|z| = 1.59$ ) and that relatively few Kougarak stations showed elevated  $\text{NO}_3\text{NO}_3^-$   
363 concentrations, despite a widespread alder presence. Increased microbial denitrification is suspected to balance  
364 increased nitrogen-fixation at these stations. This is consistent with previous studies that have noted higher nitrogen  
365 mineralization rates in acidic tundra than non-acidic tundra (Weiss et al., 2005); Kougarak is predominantly acidic  
366 tundra and Teller is non-acidic tundra.

367 The effect of vegetation on spatial variability of soil moisture was not readily observed in the volumetric moisture  
368 content of soil (Table 1 and Table 2) but was somewhat apparent in the spatial variability of moisture sensitive  
369 constituents, such as Cl (Figure 4). The lack of a clear correlation between vegetation and soil moisture by TDR or  
370 P-band SAR observations is perhaps due to the coarseness of the P-band SAR observations and the strong seasonality  
371 associated with both methods. Moisture sensitive constituents, such as Cl, may provide a more seasonally averaged  
372 tracer of soil moisture content at the stations. An increase in Cl concentrations with vegetation canopy height was  
373 apparent at Teller stations suggesting an evapotranspiration effect. This trend was also apparent at Kougarak, but the  
374 differences were rarely significant. Overall, the spatial variability of soil moisture sensitive constituents, like Cl, was  
375 far less correlated with vegetation-type than expected; perhaps due to preferential trapping of snow, which may offset  
376 the increased evapotranspiration of tall shrubs more than previously realized. Overall, Cl concentrations at Kougarak  
377 appeared to be more correlated with hillslope position than with vegetation canopy height (Figure 4).

#### 378 3.3.2.4.4 Soil Moisture and Redox Effects

379 Soil moisture content can have a profound effect on redox sensitive elements. Saturation limits oxygen diffusion into  
380 soil, and thus, forces microorganisms to utilize less energetic electron acceptors to metabolize organic matter. In an  
381 ideal system, soil microorganisms will use the strongest electron acceptor available, until it is exhausted. Although  
382 natural environments are not ideal systems, redox conditions in soils follow a more or less stepwise progression.  
383 Therefore, by evaluating the dissolved concentrations of  $\text{NO}_3\text{NO}_3^-$ , Mn, Fe, and  $\text{SO}_4\text{SO}_4^{2-}$  in SPWs, it is possible to  
384 qualitatively assess soil redox conditions and their impact on hydrogeochemical variability.

385 The redox conditions at both Teller and Kougarak are generally limited by Fe reduction, with the most reducing  
386 conditions found at stations with the highest soil moisture content. As such,  $\text{NO}_3\text{NO}_3^-$  concentrations are generally  
387 low (Table 3),  $\text{SO}_4\text{SO}_4^{2-}$  concentrations are relatively consistent (Figure 4), and Mn and Fe concentrations increase  
388 with increasing soil moisture (Figure 4).  $\text{NO}_3\text{NO}_3^-$  concentrations were generally low, except for drier stations in the  
389 proximity of tall alders or willows. While  $\text{NO}_3\text{NO}_3^-$  inputs are discussed in the vegetation effects section, the lack of  
390 high  $\text{NO}_3\text{NO}_3^-$  concentrations at wetter stations that contain alders suggests that soil moisture coupled with microbial  
391 denitrification exerts a strong control on SPW  $\text{NO}_3\text{NO}_3^-$  concentrations. Meanwhile,  $\text{SO}_4\text{SO}_4^{2-}$  concentrations at both  
392 sites are relatively constant across clear moisture and redox gradients (Figure 4). This suggests that  $\text{SO}_4\text{SO}_4^{2-}$   
393 reduction is not pervasive at either site. Dissolved Fe concentrations were higher at stations with higher soil moisture

Formatted: Not Superscript/ Subscript

Formatted: Superscript

394 content, consistent with Fe reduction. Similarly, Mn concentrations were slightly elevated at wetter stations. The  
395 concentrations of Mn, however, rarely rose above 0.05 mg·L<sup>-1</sup>, suggesting either Mn solubility limitations or a lack  
396 of a significant Mn weathering source. Low Mn concentrations at Teller Station 5, a wetter station on the upper  
397 shoulder of the Teller watershed (**Table 1; Figure 2**) seems to support the latter conclusion, as do geochemical  
398 modelling exercises (Section 4.5). Together, these results suggest that the most reducing condition at both sites is  
399 typically limited to Fe reduction and that this only occurs at stations with the highest soil moisture contents.

#### 400 **4.43.3.3 Weathering, Water/Soil Interaction, and Hydrological Transport Effects**

401 A combination of weathering, water/soil interactions, and hydrological transport were ~~clear-identified as probable~~  
402 drivers of hydrogeochemical variability for some solutes. As noted by Philben et al. (2020), soil derived solutes tend  
403 to accumulate in low-lying areas within watersheds. This is ~~clearly-seenobserved~~ at Teller, where the concentrations  
404 of Ca, Sr, and Mg all increase dramatically at the transition from lower backslope to footslope (**Figure 5**). Both Teller  
405 and Kougarok are underlain by carbonate-rich metamorphic facies, and Ca, Sr, and Mg are probable carbonate counter-  
406 cations. Weathering of Ca, Sr, and Mg carbonates and subsequent transport of these cations downslope explains this  
407 pattern of spatial variability. At Kougarok, concentrations of Ca, Mg, and Sr similarly increase from upper backslope  
408 to footslope, but concentrations of Ca and Sr decrease further down the lower backslope (Stations 10 and 1), while  
409 Mg concentrations continue to increase. A possible explanation for this behaviour is the greater affinity of cation  
410 exchange surfaces for Ca and Sr compared to Mg, thus, Ca and Sr are preferentially retained in the footslope whilst  
411 Mg is transported further down the lower backslope (Sparks, 2003, p. 189).

#### 412 **4.53.3.4 Mineral Solubility Effects**

413 Although redox reactions are rarely at equilibrium in natural environments, comparison of field data with equilibrium  
414 models provides valuable semi-quantitative insight into the redox condition of natural environments. Because Fe  
415 appeared to be limiting the development of more reducing conditions (Section 4.3), select samples from both sites  
416 were measured for soluble Fe<sup>2+</sup> following methods presented in Viollier et al. (2000). These concentrations of aqueous  
417 Fe<sup>2+</sup> were then compared with model-predicted concentrations of Fe<sup>2+</sup>, when coupled with an infinite Fe(OH)<sub>3(am)</sub>  
418 phase, across a range of pH values (2 – 10) and fixed E<sub>H</sub> values of 400 mV, 200 mV, 0 mV, and -200 mV; activity  
419 coefficients were assumed to be equal to 1. The measured and modelled Fe<sup>2+</sup> concentrations are compared in **Figure**  
420 **6**, where concentrations that were below the method detection limit (0.05 mg·L<sup>-1</sup>) are set equal to 0.025 mg·L<sup>-1</sup> (half  
421 the detection limit). Comparison of model predicted Fe<sup>2+</sup> concentrations with field data suggests that while Teller  
422 exhibits a narrower range of pH conditions than Kougarok, it exhibits a broader range of redox conditions (**Figure 6**).  
423 Although several Fe<sup>2+</sup> measurements were below the detection limit, suggesting oxidizing conditions, high Fe<sup>2+</sup>  
424 concentrations in some samples suggested E<sub>H</sub> values below 0 mV. Therefore, Fe redox conditions at Teller ranged  
425 from mildly reducing to oxic and Fe redox conditions at Kougarok ranged from mildly oxic to oxic. Oxidation-  
426 reduction potentials (ORPs), calculated from pH, Fe<sup>2+</sup> concentrations, and the Nernst equation suggest that ORPs at  
427 Teller were as low as -69 mV, while the lowest ORP at Kougarok was +134 mV (**Figure 6**). Maximum ORP values  
428 could not be determined quantitatively as some Fe<sup>2+</sup> concentrations were below Fe<sup>2+</sup> detection limits, at both sites.

429 E<sub>H</sub>/pH predominance diagrams were created from the 25th, 50th, and 100th concentration percentiles and are shown  
430 in **Figure 7** for the COIs where precipitation of mineral phases were predicted under some conditions. The  
431 concentrations for these diagrams were taken from filtered aqueous concentration data, thus, predicted mineral  
432 precipitation is an indication of nearly saturated or over-saturated conditions. The range of E<sub>H</sub> and pH conditions  
433 observed at Teller and Kougarok are overlaid as solid yellow and solid blue lines, respectively. Only the predominance  
434 diagrams that indicated possible mineral formation under the E<sub>H</sub>/pH conditions present at either site are shown in  
435 **Figure 7**. These phases included Fe(OH)<sub>3(am)</sub> (Fe), siderite (Fe), Al(OH)<sub>3(am)</sub> (Al), chalcedony (Si), barite (Ba and  
436 SO<sub>4</sub>), calcite (Ca), dolomite (Ca and Mg), and rhodochrosite (Mn). Predominance diagrams for the remaining key  
437 COIs that were not predicted to form any mineral phases under any site conditions are given in **Supplementary Figure**  
438 **4**.

439 -To further examine which mineral phases could be controlling ~~solute generation processes~~ **SPW solute concentrations**,  
440 saturated conditions for the mineral phases identified in **Figure 7** were modelled using sweeps of pH values from 2 –  
441 10 at various fixed E<sub>H</sub> values (400mV, 200mV, 0mV, and -200mV). Predicted solute concentrations under the  
442 modelled saturated conditions were then compared with field data to find common trends. In general, if solute  
443 concentrations were frequently measured near the saturation of a mineral, or were identified to have similar  
444 dependence on pH or E<sub>H</sub>, it was inferred that the mineral phase could be controlling the generation of that solute. The  
445 mineral phases that were identified to possibly be controlling solute concentrations were Al(OH)<sub>3(am)</sub>, Fe(OH)<sub>3(am)</sub>,  
446 chalcedony, and barite. This does not preclude the presence of significant concentrations of other mineral phases, it  
447 only identifies these as ~~likely possibly~~ controlling the dissolved concentrations of Al, Fe, Si, and Ba, respectively.  
448 Although it does not provide mineralogical information, X-ray fluorescence (XRF) data reported by another study at  
449 Teller confirmed high concentrations of Al, Fe, Si, and Ba in the organic and mineral soil layers at that site (Graham  
450 et al., 2018). We are unaware of any similar studies at Kougarok, nor are we aware of any studies that provide would  
451 provide confirmatory mineralogical information, for example by X-ray diffraction (XRD).

452 Aluminium concentrations in SPWs at both Teller and Kougarok appear to be controlled by the  
453 dissolution/precipitation of amorphous Al hydroxide (Al(OH)<sub>3(am)</sub>) (**Figure 8**). The solubility limit of Al(OH)<sub>3(am)</sub> has  
454 no redox dependence, but is highly pH dependent. Aluminium concentrations were generally clustered near the  
455 solubility limit of Al(OH)<sub>3(am)</sub>; Al(OH)<sub>3(am)</sub> + 3H<sup>+</sup> ↔ Al<sup>3+</sup> + 3H<sub>2</sub>O; log k = 10.8. This suggests that Al SPW  
456 concentrations at both sites are controlled by wetting/drying (dissolution/precipitation) processes. It also suggests that  
457 there could be a significant amount of Al(OH)<sub>3(am)</sub> in the soils at both sites. While organic matter may also sorb to  
458 alumina surfaces, the adherence to the solubility of Al(OH)<sub>3(am)</sub> suggests that significant concentrations of Al are not  
459 complexed with dissolved organic matter. The predominance diagrams highlight 1) the strong pH dependence on the  
460 stability of Al(OH)<sub>3(am)</sub>, 2) the influence of dissolved F can have on Al speciation when Al concentrations are low,  
461 and 3) that Al is a cation at low pH and an anion at high pH (**Figure 7**). Despite being a weathering product, Al  
462 concentrations show a dissimilar downslope trend to other weathering products, especially at Teller (**Supplementary**  
463 **Figure 5**). While the concentrations of weathering products generally increase with distance downslope, Al  
464 concentrations decrease. We suspect this can be attributed to increasing pH with distance downslope. Philben et al.  
465 (2020) reported a 1 pH unit increase in pH in organic soils along the Teller transect (**Figure 2**), increasing from 5.6 at

Formatted: Font: Bold

Formatted: Font: Bold

466 Station 5 to 6.7 at Station 9. Such an increase would decrease the solubility of  $\text{Al(OH)}_{3(\text{am})}$ , and thus, decrease the  
467 concentration of dissolved Al (**Figure 8**).

468 Similar to Al, Fe concentrations in SPWs at both Teller and Kougark appear to be controlled by the  
469 dissolution/precipitation of amorphous Fe hydroxide ( $\text{Fe(OH)}_{3(\text{am})}$ ). Fe concentrations were generally clustered near  
470 the solubility limit of  $\text{Fe(OH)}_{3(\text{am})}$  (**Figure 8**). Unlike  $\text{Al(OH)}_{3(\text{am})}$  however,  $\text{Fe(OH)}_{3(\text{am})}$  solubility is dependent on the  
471 redox condition in addition to the pH;  $\text{Fe(OH)}_{3(\text{am})} + 3\text{H}^+ + \text{e}^- \leftrightarrow \text{Fe}^{2+} + 3\text{H}_2\text{O}$ ;  $\log k = 16.0$  (**Figure 8**). Fe(III) is only  
472 sparingly soluble in aqueous solutions and reduction to Fe(II) significantly increases the solubility of Fe, thus, at a  
473 given pH value higher aqueous concentrations are predicted and observed under more reducing conditions (**Figure 8**).  
474 Iron concentrations in SPWs at both sites generally follow the pH dependence of  $\text{Fe(OH)}_{3(\text{am})}$  solubility (**Figure 8**).  
475 This suggests that SPW concentrations of Fe at both sites are controlled by wetting/drying (dissolution/precipitation)  
476 processes, coupled with the redox condition.

477 Si concentrations are frequently limited by the solubility of chalcedony, a very finely grained form of  $\text{SiO}_2$ , which is  
478 much more soluble than quartz;  $\text{SiO}_2 + 2\text{H}_2\text{O} \leftrightarrow \text{H}_4\text{SiO}_4$ ;  $\log k = -3.55$ . Particularly at Kougark, the dissolved Si  
479 concentrations, coupled with a lack of a strong pH or  $E_{\text{H}}$  dependence, suggest a controlling influence of chalcedony.

480 Ba concentrations also appear to be controlled by solubility, but rather than by the solubility of an oxide or a hydroxide  
481 phase, by the solubility of barite [ $\text{Ba}^{2+} + \text{SO}_4^{2-} \leftrightarrow \text{BaSO}_4(\text{s})$ ;  $\log k = 9.97$ ]. Unlike Al hydroxide or Fe hydroxide, barite  
482 solubility lacks a strong pH dependence and instead is dependent solely on the activities of  $\text{Ba}^{2+}$  and  $\text{SO}_4^{2-}$ . Unlike Ba,  
483  $\text{SO}_4\text{SO}_3^{2-}$  concentrations are not limited by the solubility limit of barite and are generally higher and not well correlated  
484 with Ba concentrations. Together, these suggest that  $\text{SO}_4\text{SO}_3^{2-}$  from another source (likely, atmospheric deposition or  
485 sulfidic mineral oxidation), is suppressing barite dissolution, and thus, is reducing dissolved Ba concentrations. Barite  
486 solubility can exhibit a redox dependence if conditions are sufficiently reducing to reduce  $\text{SO}_4\text{SO}_3^{2-}$  to sulphide (Neff,  
487 2002). This shifts the equilibrium to greater dissolution of barite, and therefore higher conditions of Ba. The lack of  
488  $E_{\text{H}}$  dependence in observational data further suggests that neither site exhibits significant  $\text{SO}_4\text{SO}_3^{2-}$  reduction.

#### 489 **5.4. Conclusions Discussion**

490 The 18 stations examined herein (8 at Teller and 10 at Kougark) represent a wide range of vegetation types, soil  
491 moisture contents, permafrost extents, and hillslope positions. Coupling the spatial variability of these landscape  
492 characteristics with the spatial variability of SPW solute concentrations provides valuable insight into the dominant  
493 environmental controls on observed spatial variability of SPW geochemistry. It is our hope that correlating SPW  
494 geochemistry with readily observable and scalable landscape features will inform earth system modelling efforts in  
495 permafrost regions and provide fast and easy methods to determine if earth system models are working properly (i.e.  
496 predicting the correct trends). The inferred dominant environmental controls on the observed inter-site and intra-site  
497 variability of SPW solute concentrations are discussed in the following sections.

Formatted: Subscript

498 **4.1 The Dominant Environmental Controls on Inter-site Variability of SPW Solute Concentrations**

499 Overall, the more frequent instance of significantly greater constituent concentrations at Kougarok suggests a  
500 systematic cause. The extensive low-gradient toeslope (Figure 2) and lack of a well-defined drainage channel at  
501 Kougarok, are likely causes of the systematically higher SPW solute concentrations at Kougarok. Water perching, the  
502 result of near-surface permafrost in the lower-backslope and toeslope, is likely to increase evapotranspiration and,  
503 thus, SPW solute concentrations. Significant evapotranspiration caused by supra-permafrost water table perching has  
504 been noted in several previous studies (Huang et al., 2022; Park et al., 2021; Sjöberg et al., 2021). Meanwhile, the  
505 lack of a drainage channel at Kougarok suggests that runoff (and therefore solute exports) is more limited than at  
506 Teller. Without a relatively rapid export mechanism such as a stream channel, solute transport is likely limited to  
507 interflow within the Kougarok hillslope over much of the thaw season, allowing weathering products to increase to  
508 significantly greater concentrations than those observed at Teller, where a well-defined drainage/export mechanism  
509 does exist. Field observations from pits at Kougarok confirm observable interflow at the site. Overall, our study  
510 suggests that evaporative concentration could be a significant control on SPW solute concentrations in permafrost  
511 catchments, especially in those with limited drainage and therefore a perched near-surface water table. This effect has  
512 been reported previously (Raudina et al., 2017), but does not appear to be widely considered, perhaps due to the  
513 generally few studies of SPW solutes in permafrost regions. We suggest future efforts to predict future SPW solute  
514 and nutrient dynamics directly address the impacts of evaporative concentration on permafrost catchments, especially  
515 with future permafrost thaw.

516 The exception to the general observation of elevated concentrations at Kougarok versus Teller was  $\text{SO}_4^{2-}$ . Although  
517 the cause of consistently higher  $\text{SO}_4^{2-}$  concentrations at Teller is unclear from the limited scope of this study, it seems  
518 likely to be due to a greater abundance of sulfidic bedrock material. The presence of sulfidic bedrock in the vicinity  
519 of Teller has been reported by mineral prospecting efforts (Brobst, Pinckney, and Sainsbury, 1971; Herreid, 1966;  
520 Mulligan, 1965); we are unaware of any such reports near Kougarok. It should be recognized  $\text{SO}_4^{2-}$  concentrations at  
521 both Kougarok and Teller are relatively low.

Formatted: Normal

523 **4.5.12 The Dominant Environmental Controls on Intra-site Spatial Variability of SPW Solute Concentrations**

524 The 18 stations examined herein (8 at Teller and 10 at Kougarok) were selected to represent a wide range of vegetation  
525 types, soil moisture contents, permafrost extents, and hillslope positions. Coupling the spatial variability of these  
526 landscape characteristics with the spatial variability of SPW solute concentrations provides valuable insight into the  
527 dominant environmental controls on observed spatial variability of SPW geochemistry.

528 With regard to our initial hypotheses, our major findings are that:

529 Vegetation influences on elemental cycles were only readily apparent for nitrogen and although vegetation induced  
530 changes to soil moisture content were discernible, they were far less significant than anticipated.  $\text{NO}_3\text{NO}_2^-$  was the  
531 only COI that exhibited a clear vegetation effect; elevated concentrations were associated with the presence of alder  
532 shrubs and, in some cases, tall willow shrubs. These increases in  $\text{NO}_3\text{NO}_2^-$  concentrations associated with alder

Formatted: Subscript

Formatted: Subscript

533 nitrogen-fixation and the mineralization and nitrification of willow leaf litter were frequently equipoised by increased  
534 microbial denitrification in regions sufficiently moist to support it, this is perhaps one of the most significant findings  
535 of this work. –Although both Kougarok and Teller exhibited some indications of increased Cl concentrations in the  
536 presence of tall shrubs, the net vegetation effect on soil moisture was far less than hypothesized. Redox sensitivity  
537 was also less than ~~hypothesized~~hypothesized, and most stations seemed well-buffered at Fe redox conditions. The  
538 result of this buffering was generally low  $\text{NO}_2\text{NO}_3^-$  concentrations (except where vegetation effects dominated),  
539 consistent  $\text{SO}_4\text{SO}_4^{2-}$  concentrations across clear redox gradients, and variable Mn and Fe concentrations. Mn  
540 concentrations were generally low, likely due to a limited source. Fe concentrations were higher at stations with higher  
541 soil moisture content, consistent with Fe reduction. Similar Fe redox cycling between soluble Fe(II) species and  
542 precipitated Fe oxyhydroxides in permafrost catchments has been reported recently (Patzner et al., 2022), which  
543 suggests that Fe redox buffering in permafrost landscapes is widespread. Weathering, water/soil interactions, and  
544 hydrological transport were ~~clear~~probable drivers of variability for Ca, Sr, and Mg. Ca, Sr, and Mg all tended to  
545 accumulate in low-lying areas, although Ca and Sr demonstrated greater accumulation potential than Mg, likely via  
546 greater affinity of cation exchange surfaces for Ca and Sr compared to Mg. Mineral solubility limitations were the  
547 primary controls on Al ( $\text{Al}(\text{OH})_{3(\text{am})}$ ), Fe ( $\text{Fe}(\text{OH})_{3(\text{am})}$ ), Ba (barite), and Si (chalcedony) concentrations. This suggests  
548 that the SPW concentrations of these constituents will remain stable until those mineral phases are exhausted or soil  
549 pore hydrochemistry changes sufficiently to alter the solubility of those mineral phases. Supersaturation of Al with  
550 respect to gibbsite (crystalline  $\text{Al}(\text{OH})_3$ ) and Si with respect to chalcedony in a permafrost wetland has been reported  
551 previously (Jesson et al., 2014). The solubility curves for gibbsite and  $\text{Al}(\text{OH})_{3(\text{am})}$  are similar, with  $\text{Al}(\text{OH})_{3(\text{am})}$  being  
552 slightly more soluble at all pH values due to the increased thermodynamic stability of the crystalline Al hydroxide  
553 mineral, gibbsite. Meanwhile, seasonal precipitation of Fe oxyhydroxides in permafrost peatlands and their effect of  
554 carbon cycling was the subject of an excellent paper by Patzner et al. (2022). Our study is the first observation we are  
555 aware of that reports the saturation controls of barite on Ba in permafrost SPWs, although that could be because  
556 relatively few studies consider barium concentrations; it is worthwhile emphasizing that Ba was not supersaturated  
557 with respect to barite but approached a saturated condition. Future studies should also note that C changes in redox  
558 condition would significantly alter  $\text{Fe}(\text{OH})_{3(\text{am})}$  solubility, whereas changes in pH conditions would significantly alter  
559  $\text{Al}(\text{OH})_{3(\text{am})}$  and  $\text{Fe}(\text{OH})_{3(\text{am})}$  solubility.

560 Although discerning the environmental controls on spatial variability of SPW solute concentrations provides some  
561 high-level insight into the effects changes in landscape character may have on soil pore hydrochemistry, our scope  
562 was limited and leveraged on previously available datasets. The significance of SPW in small Arctic headwater  
563 catchments as a key initial component in the freshwater hydrologic continuum is under recognized, and such  
564 catchments warrant more detailed and systematic investigations.

Formatted: Subscript

Formatted: Subscript

## 566 **56. Acknowledgements**

567 We would like to thank the Sitnasuak Native Corporation and the Mary's Igloo Native Corporation for their guidance  
568 and for allowing us to conduct this research on the traditional homelands of the Inupiat people. Funding was provided



569 by the Next-Generation Ecosystem Experiments (NGEE Arctic) project, supported by the Office of Biological and  
570 Environmental Research in the U.S. DOE Office of Science. We wish to thank Lauren Charsley-Groffman and Nathan  
571 Wales for their assistance with fieldwork, as well as, George Perkins, Oana Marina, Rose Harris, and Emily Kluk for  
572 their assistance with laboratory analyses.

#### 573 **76. Data availability statement**

574 The data that support the findings of this study are made openly available in the NGEE-Arctic data repository at (DOI:  
575 10.5440/1735757).

#### 576 **87. References**

- 577 [Anderson, M. D., Ruess, R. W., Myrold, D. D., and Taylor, D. L. \(2009\). Host species and habitat affect nodulation](#)  
578 [by specific Frankia genotypes in two species of Alnus in interior Alaska. \*Oecologia\* 160, 619–630. doi:](#)  
579 [10.1007/s00442-009-1330-0](#)
- 580 [Anderson, M. D., Ruess, R. W., Uliassi, D. D., and Mitchell, J. S. \(2004\). Estimating N<sub>2</sub> fixation in two species of](#)  
581 [Alnus in interior Alaska using acetylene reduction and 15N<sub>2</sub> uptake. \*Ecoscience\* 11, 102–112. doi: 10.1080/](#)  
582 [11956860.2004.11682814](#)
- 583 [Binkley, D., Sollins, P., Bell, R., Sachs, D., and Myrold, D.: Biogeochemistry of adjacent conifer and alder-conifer](#)  
584 [stands, \*Ecology\*, 73, 2022–2033, 1992.](#)
- 585 Breen, A., Iversen, C., Salmon, V., VanderStel, H., Busey, B., and Wulschleger, S. 2020a:. NGEE Arctic Plant Traits:  
586 Plant Community Composition, Kougarak Road Mile Marker 64, Seward Peninsula, Alaska, 2016 [Data set], doi:  
587 <https://doi.org/10.5440/1465967>.
- 588 Breen, A., Iversen, C., Salmon, V., VanderStel, H., Busey, B., and Wulschleger, S. 2020b:. NGEE Arctic Plant Traits:  
589 Plant Community Composition, Kougarak Road Mile Marker 64, Seward Peninsula, Alaska, 2016 [Data set], doi:  
590 <https://doi.org/10.5440/1465967>.
- 591 Bring, A., Fedorova, I., Dibike, Y., Hinzman, L., Mård, J., Mernild, S. H., ... Woo, M.-K. 2016: Arctic terrestrial  
592 hydrology: A synthesis of processes, regional effects, and research challenges. *Journal of Geophysical Research:*  
593 *Biogeosciences*, 121: 621–649, doi: <https://doi.org/10.1002/2015JG003131>.
- 594 Brobst, D. A., Pinckney, D. M., and Sainsbury, C. L. 1971: Geology and Geochemistry of the Sinuk River Barite  
595 Deposit, Seward Peninsula, Alaska (No. 463 (?)). United States Department of the Interior Geological Survey.
- 596 [Bühlmann, T., Hiltbrunner, E., and Körner, C.: Alnus viridis expansion contributes to excess reactive nitrogen release,](#)  
597 [reduces biodiversity and constrains forest succession in the Alps. \*Alpine Botany\*, 124, 187–191,](#)  
598 <https://doi.org/10.1007/s00035-014-0134-y>, 2014.
- 599 [Clein, J. S. and Schimel, J. P.: Nitrogen turnover and availability during succession from alder to poplar in Alaskan](#)  
600 [taiga forests, \*Soil Biology and Biochemistry\*, 27, 743–752, \[https://doi.org/10.1016/0038-0717\\(94\\)00232-P\]\(https://doi.org/10.1016/0038-0717\(94\)00232-P\), 1995.](#)

601 Conroy, N., Heikoop, J., Newman, B., Wilson, C., Arendt, C., Perkins, G., and Wullschleger, S. 2021: Soil Water  
602 Chemistry and Water and Nitrogen Isotopes, Teller Road Site and Kougarok Hillslope, Seward Peninsula, Alaska,  
603 2016 - 2019 [Data set], doi: <https://doi.org/10.5440/1735757>.

604 Corder, G. W., and Foreman, D. I. 2009: Nonparametric statistics for non-statisticians: a step-by-step approach.  
605 Hoboken, N.J.; Wiley, 247 pp.

606 Frey, K. E., and McClelland, J. W. 2009: Impacts of permafrost degradation on arctic river biogeochemistry.  
607 Hydrological Processes, 23: 169–182, doi: <https://doi.org/10.1002/hyp.7196>.

608 Frisbee, M. D., Phillips, F. M., Campbell, A. R., and Hendrickx, J. M. H. 2010: Modified passive capillary samplers  
609 for collecting samples of snowmelt infiltration for stable isotope analysis in remote, seasonally inaccessible  
610 watersheds 1: laboratory evaluation. Hydrological Processes, 24: 825–833, doi: <https://doi.org/10.1002/hyp.7523>.

611 Fuchs, M., Nitze, I., Strauss, J., Günther, F., Wetterich, S., Kizyakov, A., ... Grosse, G. 2020: Rapid Fluvio-Thermal  
612 Erosion of a Yedoma Permafrost Cliff in the Lena River Delta. *Frontiers in Earth Science*, 8: 336, doi:  
613 <https://doi.org/10.3389/feart.2020.00336>.

614 Graham, D. E., Kholodov, A., Wilson, C. J., Moon, J.-W., Romanovsky, V. E., and Busey, B. 2018: Soil Physical,  
615 Chemical, and Thermal Characterization, Teller Road Site, Seward Peninsula, Alaska, 2016., doi:  
616 <https://doi.org/10.5440/1342956>.

617 Harms, T. K., and Jones, J. B. 2012: Thaw depth determines reaction and transport of inorganic nitrogen in valley  
618 bottom permafrost soils. *Global Change Biology*, 18: 2958–2968, doi: [https://doi.org/10.1111/j.1365-](https://doi.org/10.1111/j.1365-619)  
619 [2486.2012.02731.x](https://doi.org/10.1111/j.1365-2486.2012.02731.x).

620 Harms, T. K., and Ludwig, S. M. 2016: Retention and removal of nitrogen and phosphorus in saturated soils of arctic  
621 hillslopes. *Biogeochemistry*, 127: 291–304, doi: <https://doi.org/10.1007/s10533-016-0181-0>.

622 Helsel, D. R. 2005: Nondetects and data analysis: statistics for censored environmental data. Hoboken, NJ.; Wiley-  
623 Interscience, 250 pp.

624 Herreid, G. 1966: Preliminary geology and geochemistry of the Sinuk River area. Seward Peninsula, Alaska: Alaska  
625 Division of Mines and Minerals Geologic Report, 24: 19.

626 Hiyama, T., Yang, D. and Kane, D.L., 2021. Permafrost Hydrology: Linkages and Feedbacks. In *Arctic Hydrology,*  
627 *Permafrost and Ecosystems* (pp. 471-491). Springer, Cham.

628 [Hollingsworth, T. N., Lloyd, A. H., Nossov, D. R., Ruess, R. W., Charlton, B. A., and Kielland, K. \(2010\). Twenty-](#)  
629 [five years of vegetation change along a putative successional chronosequence on the Tanana River, Alaska. \*Can. J.\*](#)  
630 [For. Res. 40, 1273–1287. doi: 10.1139/X10-094](#)

631 Hopkins, D. M., Karlstrom, T. N. V., Black, R. F., Williams, J. R., Pewe, T. L., Fernald, A. T., and Muller, E. H.  
632 1955: Permafrost and ground water in Alaska. U.S. Geological Survey Professional Paper 264-F.

633 [Huang, Q., Ma, N., & Wang, P. \(2022\). Faster increase in evapotranspiration in permafrost-dominated basins in the](#)  
634 [warming Pan-Arctic. \*Journal of Hydrology\*, 615, 128678. https://doi.org/10.1016/j.jhydrol.2022.128678](#)

635 Jafarov, E. E., Coon, E. T., Harp, D. R., Wilson, C. J., Painter, S. L., Atchley, A. L., and Romanovsky, V. E. 2018:  
636 Modelling the role of preferential snow accumulation in through talik development and hillslope groundwater flow in

637 a transitional permafrost landscape. *Environmental Research Letters*, 13: 105006, doi: <https://doi.org/10.1088/1748-9326/aadd30>.

638

639 [Jessen, Søren, Hanne D. Holmslykke, Kristine Rasmussen, Niels Richardt, and Peter E. Holm. 2014. "Hydrology and Pore Water Chemistry in a Permafrost Wetland, Ilulissat, Greenland." \*Water Resources Research\* 50 \(6\): 4760–74. <https://doi.org/10.1002/2013WR014376>.](#)

640

641

642 Kinniburgh, D., and Cooper, D. 2011: PhreePlot: Creating Graphical Output with Phreeqc.

643 Koch, J. C., Runkel, R. L., Striegl, R., and McKnight, D. M. 2013: Hydrologic controls on the transport and cycling of carbon and nitrogen in a boreal catchment underlain by continuous permafrost. *Journal of Geophysical Research: Biogeosciences*, 118: 698–712, doi: <https://doi.org/10.1002/jgrg.20058>.

644

645

646 Kokelj, S. V., and Jorgenson, M. T. 2013: Advances in Thermokarst Research. *Permafrost and Periglacial Processes*, 24: 108–119, doi: <https://doi.org/10.1002/ppp.1779>.

647

648 Kurylyk and Walvoord, 2021 Kurylyk, B.L. and Walvoord, M.A., 2021. Permafrost Hydrogeology. In *Arctic Hydrology, Permafrost and Ecosystems* (pp. 493-523). Springer, Cham.

649

650 [Langford, Z. L., Kumar, J., Hoffman, F. M., Breen, A. L., & Iversen, C. M. \(2019\). Arctic vegetation mapping using unsupervised training datasets and convolutional neural networks. \*Remote Sensing\*, 11\(1\), 1–23. <https://doi.org/10.3390/rs11010069>](#)

651

652

653 Lara, M. J., Nitze, I., Grosse, G., and McGuire, A. D. 2018: Tundra landform and vegetation productivity trend maps for the Arctic Coastal Plain of northern Alaska. *Scientific Data*, 5: 1–10, doi: <https://doi.org/10.1038/sdata.2018.58>.

654

655 Léger, E., Dafflon, B., Robert, Y., Ulrich, C., Peterson, J. E., Biraud, S. C., ... Hubbard, S. S. 2019: A distributed temperature profiling method for assessing spatial variability in ground temperatures in a discontinuous permafrost region of Alaska. *The Cryosphere*, 13: 2853–2867, doi: <https://doi.org/10.5194/tc-13-2853-2019>.

656

657

658 Liljedahl, A. K., Boike, J., Daanen, R. P., Fedorov, A. N., Frost, G. V., Grosse, G., ... Zona, D. 2016: Pan-Arctic ice-wedge degradation in warming permafrost and its influence on tundra hydrology. *Nature Geoscience*, 9: 312–318, doi: <https://doi.org/10.1038/ngeo2674>.

659

660

661 [McCaully, R. E., Arendt, C. A., Newman, B. D., Salmon, V. G., Heikoop, J. M., Wilson, C. J., Sevanto, S., Wales, N. A., Perkins, G. B., Marina, O. C., and Wullschleger, S. D.: High nitrate variability on an Alaskan permafrost hillslope dominated by alder shrubs. \*The Cryosphere\*, 16, 1889–1901. <https://doi.org/10.5194/tc-16-1889-2022>, 2022.](#)

662

663

664 [McCaully, R. E., Arendt, C. A., Newman, B. D., Heikoop, J. M., Wilson, C. J., Sevanto, S., ... Wullschleger, S. D. In Review.: High Temporal and Spatial Nitrate Variability on an Alaskan Hillslope Dominated by Alder Shrubs. \*The Cryosphere\*.](#)

665

666

667 McClelland, J. W., Holmes, R. M., Peterson, B. J., Raymond, P. A., Striegl, R. G., Zhulidov, A. V., ... Griffin, C. G. 2016: Particulate organic carbon and nitrogen export from major Arctic rivers. *Global Biogeochemical Cycles*, 30: 629–643, doi: <https://doi.org/10.1002/2015GB005351>.

668

669

670 [Mitchell, J. S., and Ruess, R. W. \(2009\). N2 fixing alder \(\*Alnus viridis\* spp. \*fruticosa\*\) effects on soil properties across a secondary successional chronosequence in interior Alaska. \*Biogeochemistry\* 95, 215–229. doi: 10.1007/s10533-009-9332-x](#)

671

672

673 Mulligan, J. J. 1965: Examination of the Sinuk Iron Deposits Seward Peninsula, Alaska. United States Department of  
674 the Interior, 37.

675 Myers-Smith, I. H., Forbes, B. C., Wilmsking, M., Hallinger, M., Lantz, T., Blok, D., ... Hik, D. S. 2011: Shrub  
676 expansion in tundra ecosystems: dynamics, impacts and research priorities. *Environmental Research Letters*, 6:  
677 045509, doi: <https://doi.org/10.1088/1748-9326/6/4/045509>.

678 [Neff, J. \(2002\). Barium in the Ocean. In \*Bioaccumulation in Marine Organisms\* \(pp. 79–87\).](#)

679 [Nossov, D. R., Hollingsworth, T. N., Ruess, R. W., and Kielland, K. \(2011\). Development of \*Alnus tenuifolia\* stands  
680 on an Alaskan floodplain: patterns of recruitment, disease and succession. \*J. Ecol.\* 99, 621–633. doi: 10.1111/j.1365-  
681 2745.2010.01792.x](#)

682 O'Donnell, J., Douglas, T., Barker, A. and Guo, L., 2021. Changing Biogeochemical Cycles of Organic Carbon,  
683 Nitrogen, Phosphorus, and Trace Elements in Arctic Rivers. In *Arctic Hydrology, Permafrost and Ecosystems* (pp.  
684 315-348). Springer, Cham.

685 [Patzner, M.S., Kainz, N., Lundin, E., Barczok, M., Smith, C., Herndon, E., Kinsman-Costello, L., Fischer, S., Straub,  
686 D., Kleindienst, S., Kappler, A., Bryce, C., 2022. Seasonal Fluctuations in Iron Cycling in Thawing Permafrost  
687 Peatlands. \*Environ. Sci. Technol.\* 56, 4620–4631. <https://doi.org/10.1021/acs.est.1c06937>](#)

688 [Park, H., Tanoue, M., Sugimoto, A., Ichiyonagi, K., Iwahana, G., & Hiyama, T. \(2021\). Quantitative Separation of  
689 Precipitation and Permafrost Waters Used for Evapotranspiration in a Boreal Forest: A Numerical Study Using Tracer  
690 Model. \*Journal of Geophysical Research: Biogeosciences\*, 126\(12\). <https://doi.org/10.1029/2021JG006645>](#)

691 Parkhurst, D., and Appelo, C. A. J. 2013: Description of input and examples for PHREEQC version 3: a computer  
692 program for speciation, batch-reaction, one-dimensional transport, and inverse geochemical calculations (USGS  
693 Numbered Series No. 6-A43). Reston, VA: U.S. Geological Survey.

694 Perdrial, J. N., Perdrial, N., Vazquez-Ortega, A., Porter, C., Leedy, J., and Chorover, J. 2014: Experimental  
695 Assessment of Passive Capillary Wick Sampler Suitability for Inorganic Soil Solution Constituents. *Soil Science  
696 Society of America Journal*, 78: 486–495, doi: <https://doi.org/10.2136/sssaj2013.07.0279>.

697 Petrone, K. C., Hinzman, L. D., Shibata, H., Jones, J. B., and Boone, R. D. 2007: The influence of fire and permafrost  
698 on sub-arctic stream chemistry during storms. *Hydrological Processes*, 21: 423–434, doi:  
699 <https://doi.org/10.1002/hyp.6247>.

700 Philben, M., Taş, N., Chen, H., Wullschleger, S. D., Kholodov, A., Graham, D. E., and Gu, B. 2020: Influences of  
701 hillslope biogeochemistry on anaerobic soil organic matter decomposition in a tundra watershed. *Journal of  
702 Geophysical Research: Biogeosciences*, n/a: e2019JG005512, doi: <https://doi.org/10.1029/2019JG005512>.

703 Philben, M., Zheng, J., Bill, M., Heikoop, J. M., Perkins, G., Yang, Z., ... Gu, B. 2019: Stimulation of anaerobic  
704 organic matter decomposition by subsurface organic N addition in tundra soils. *Soil Biology and Biochemistry*, 130:  
705 195–204, doi: <https://doi.org/10.1016/j.soilbio.2018.12.009>.

706 Prowse, T., Bring, A., Mård, J., and Carmack, E. 2015: Arctic Freshwater Synthesis: Introduction. *Journal of  
707 Geophysical Research: Biogeosciences*, 120: 2121–2131, doi: <https://doi.org/10.1002/2015JG003127>.

Formatted: Normal

708 Prowse, T., Bring, A., Mård, J., Carmack, E., Holland, M., Instanes, A., ... Wrona, F. J. 2015: Arctic Freshwater  
709 Synthesis: Summary of key emerging issues. *Journal of Geophysical Research: Biogeosciences*, 120: 1887–1893, doi:  
710 <https://doi.org/10.1002/2015JG003128>.

711 R Core Team. 2020: R: A Language and Environment for Statistical Computing. Vienna, Austria., R Foundation for  
712 Statistical Computing. Retrieved from <https://www.R-project.org/>.

713 [Raudina, Tatiana V., Sergey V. Loiko, Artyom G. Lim, Ivan V. Krickov, Liudmila S. Shirokova, Georgy I. Istigechev,](#)  
714 [Daria M. Kuzmina, Sergey P. Kulizhsky, Sergey N. Vorobyev, and Oleg S. Pokrovsky. 2017. "Dissolved Organic](#)  
715 [Carbon and Major and Trace Elements in Peat Porewater of Sporadic, Discontinuous, and Continuous Permafrost](#)  
716 [Zones of Western Siberia." \*Biogeosciences\* 14 \(14\): 3561–84. <https://doi.org/10.5194/bg-14-3561-2017>.](#)

717 [Raynolds, M.K.; Walker, D.A.; Maier, H.A. Plant community-level mapping of arctic Alaska based on the](#)  
718 [Circumpolar Arctic Vegetation Map. \*Phytocoenologia\* 2005, 35, 821–848.](#)

719 [Raynolds, M. K., Walker, D. A., Balseer, A., Bay, C., Campbell, M., Cherosov, M. M., et al. \(2019\). A raster version](#)  
720 [of the Circumpolar Arctic Vegetation Map \(CAVM\). \*Remote Sensing of Environment\*, 232.](#)  
721 <https://doi.org/10.1016/j.rse.2019.111297>

722 Romanovsky, V., Cable, W., and Dolgikh, K. 2020a.: Soil Temperature and Moisture, Kougarak Road Mile Marker  
723 64, Seward Peninsula, Alaska, beginning 2016 [Data set], doi: <https://doi.org/10.5440/1581586>.

724 Romanovsky, V., Cable, W., and Dolgikh, K. 2020b.: Soil Temperature and Moisture, Kougarak Road Mile Marker  
725 64, Seward Peninsula, Alaska, beginning 2016 [Data set], doi: <https://doi.org/10.5440/1581586>.

726 Romanovsky, V., Cable, W., and Dolgikh, K. 2020c.: Soil Temperature and Moisture, Teller Road Mile Marker 27,  
727 Seward Peninsula, Alaska, beginning 2016 [Data set], doi: <https://doi.org/10.5440/1581437>.

728 Romanovsky, V., Cable, W., and Dolgikh, K. 2020d.: Soil Temperature and Moisture, Teller Road Mile Marker 27,  
729 Seward Peninsula, Alaska, beginning 2016 [Data set], doi: <https://doi.org/10.5440/1581437>.

730 Rowland, J. C., Jones, C. E., Altmann, G., Bryan, R., Crosby, B. T., Hinzman, L. D., ... Geernaert, G. L. 2010: Arctic  
731 Landscapes in Transition: Responses to Thawing Permafrost. *Eos, Transactions American Geophysical Union*, 91:  
732 229–230, doi: <https://doi.org/10.1029/2010EO260001>.

733 [Ruess, R. W., Anderson, M. D., McFarland, J. M., Kielland, K., Olson, K., and Taylor, D. L. \(2013\). Ecosystem-level](#)  
734 [consequences of symbiont partnerships in an N-fixing shrub from interior Alaskan floodplains. \*Ecol. Monogr.\* 83,](#)  
735 [177– 194. doi: 10.1890/12-0782.1](#)

736 Salmon, V. G., Breen, A. L., Kumar, J., Lara, M. J., Thornton, P. E., Wulschleger, S. D., and Iversen, C. M. 2019:  
737 Alder Distribution and Expansion Across a Tundra Hillslope: Implications for Local N Cycling. *Frontiers in Plant*  
738 *Science*, 10, doi: <https://doi.org/10.3389/fpls.2019.01099>.

739 Schuur, E. A. G., McGuire, A. D., Schädel, C., Grosse, G., Harden, J. W., Hayes, D. J., ... Vonk, J. E. 2015: Climate  
740 change and the permafrost carbon feedback. *Nature*, 520: 171–179, doi: <https://doi.org/10.1038/nature14338>.

741 Shaver, G. R., Billings, W. D., Chapin, F. S., Giblin, A. E., Nadelhoffer, K. J., Oechel, W. C., and Rastetter, E. B.  
742 1992: Global Change and the Carbon Balance of Arctic Ecosystems. *BioScience*, 42: 433–441, doi:  
743 <https://doi.org/10.2307/1311862>.

744 Shogren, A. J., Zarnetske, J. P., Abbott, B. W., Iannucci, F., Frei, R. J., Griffin, N. A., and Bowden, W. B. 2019:  
745 Revealing biogeochemical signatures of Arctic landscapes with river chemistry. *Scientific Reports*, 9: 1–11, doi:  
746 <https://doi.org/10.1038/s41598-019-49296-6>.

747 [Sjöberg, Y., Jan, A., Painter, S. L., Coon, E. T., Carey, M. P., O'Donnell, J. A., & Koch, J. C. \(2021\). Permafrost](#)  
748 [Promotes Shallow Groundwater Flow and Warmer Headwater Streams. \*Water Resources Research\*, 57\(2\).](#)  
749 <https://doi.org/10.1029/2020WR027463>

750 Smith, L. C., Sheng, Y., MacDonald, G. M., and Hinzman, L. D. 2005: Disappearing Arctic Lakes. *Science*, 308:  
751 1429–1429, doi: <https://doi.org/10.1126/science.1108142>.

752 Sparks, D. L. 2003: *Environmental soil chemistry* (2nd ed). Amsterdam ; Boston:, Academic Press, 352 pp.

753 Spence, C., Kokelj, S., McCluskie, M., and Hedstrom, N. 2015: Impacts of Hydrological and Biogeochemical Process  
754 Synchrony Transcend Scale. In *AGU Fall Meeting Abstracts* (Vol. 2015).

755 Sturm, M., Racine, C., and Tape, K. 2001: Increasing shrub abundance in the Arctic. *Nature*, 411: 546–547, doi:  
756 <https://doi.org/10.1038/35079180>.

757 [Sulman, B. N., Salmon, V. G., Iversen, C. M., Breen, A. L., Yuan, F., & Thornton, P. E. \(2021\). Integrating arctic](#)  
758 [plant functional types in a land surface model using above- and belowground field observations. \*Journal of Advances\*](#)  
759 [in Modeling Earth Systems](#), 13, e2020MS002396. <https://doi.org/10.1029/2020MS002396>

760 Tape, K. D., Hallinger, M., Welker, J. M., and Ruess, R. W. 2012: Landscape Heterogeneity of Shrub Expansion in  
761 Arctic Alaska. *Ecosystems*, 15: 711–724, doi: <https://doi.org/10.1007/s10021-012-9540-4>.

762 Tape, K., Sturm, M., and Racine, C. 2006: The evidence for shrub expansion in Northern Alaska and the Pan-Arctic.  
763 *Global Change Biology*, 12: 686–702, doi: <https://doi.org/10.1111/j.1365-2486.2006.01128.x>.

764 Till, A. B., Dumoulin, J. A., Weldon, M. B., and Bleick, H. A. 2011: Bedrock geologic map of the Seward Peninsula,  
765 Alaska, and accompanying conodont data. US Department of the Interior, US Geological Survey.

766 Uren, N. C. 2018: Calcium oxalate in soils, its origins and fate – a review. *Soil Research*, 56: 443, doi:  
767 <https://doi.org/10.1071/SR17244>.

768 Vonk, J. E., Tank, S. E., Bowden, W. B., Laurion, I., Vincent, W. F., Alekseychik, P., ... Wickland, K. P. 2015:  
769 Reviews and syntheses: Effects of permafrost thaw on Arctic aquatic ecosystems. *Biogeosciences*, 12: 7129–7167,  
770 doi: <https://doi.org/10.5194/bg-12-7129-2015>.

771 Vonk, J. E., Tank, S. E., and Walvoord, M. A. 2019: Integrating hydrology and biogeochemistry across frozen  
772 landscapes. *Nature Communications*, 10: 1–4, doi: <https://doi.org/10.1038/s41467-019-13361-5>.

773 [Walker, D. A., Breen, A. L., Druckenmiller, L. A., Wirth, L. W., Fisher, W., Reynolds, M. K., Sibik, J., Walker, M.](#)  
774 [D., Hennekens, S., Boggs, K., Boucher, T., Buchhorn, M., Bultmann, H., Cooper, D. J., Daniels, F. J. A., Davidson,](#)  
775 [S. J., Ebersole, J. J., Elmendorf, S. C., Epstein, H. E., Gould, W. A., Hollister, R. D., Iversen, C. M., Jorgenson, M.](#)  
776 [T., Kade, A., Lee, M. T., MacKenzie, W. H., Peet, R. K., Peirce, J. L., Schickhoff, U., Sloan, V. L., Talbot, S. S.,](#)  
777 [Tweedie, C. E., Villarreal, S., Webber, P. J., and Zona, D.: The Alaska Arctic Vegetation Archive \(AVA-AK\).](#)  
778 [Phytocoenologia](#), 46, 221–229. <https://doi.org/10.1127/phyto/2016/0128>, 2016.

779 Wallenberger, F. T., and Bingham, P. A. 2009: *Fiberglass and Glass Technology: Energy-Friendly Compositions and*  
780 *Applications*. Springer Science & Business Media, 479 pp.

781 Walvoord, M. A., and Kurylyk, B. L. 2016: Hydrologic Impacts of Thawing Permafrost—A Review. *Vadose Zone*  
782 *Journal*, 15, doi: <https://doi.org/10.2136/vzj2016.01.0010>.

783 Weiss, M., Hobbie, S. E., & Gettel, G. M. (2005). Contrasting Responses of Nitrogen-Fixation in Arctic Lichens to  
784 Experimental and Ambient Nitrogen and Phosphorus Availability. *Arctic, Antarctic, and Alpine Research*, 37(3), 396–  
785 401. [https://doi.org/10.1657/1523-0430\(2005\)037\[0396:CRONIA\]2.0.CO;2](https://doi.org/10.1657/1523-0430(2005)037[0396:CRONIA]2.0.CO;2)

786 Wilson, C., Bolton, R., Busey, R., Lathrop, E., and Dann, J. 2019: End-of-Winter Snow Depth, Temperature, Density  
787 and SWE Measurements at Kougarak Road Site, Seward Peninsula, Alaska, 2018 [Data set], doi:  
788 <https://doi.org/10.5440/1593874>.

789 Wilson, C., Bolton, R., Busey, R., Lathrop, E., Dann, J., and Charsley-Groffman, L. 2019: End-of-Winter Snow Depth,  
790 Temperature, Density and SWE Measurements at Teller Road Site, Seward Peninsula, Alaska, 2016-2018 [Data set],  
791 doi: <https://doi.org/10.5440/1592103>.

792 Wilson, C., Dann, J., Bolton, R., Charsley-Groffman, L., Jafarov, E., Musa, D., and Wulschleger, S. 2021: In Situ  
793 Soil Moisture and Thaw Depth Measurements Coincident with Airborne SAR Data Collections, Barrow and Seward  
794 Peninsulas, Alaska, 2017 [Data set], doi: <https://doi.org/10.5440/1423892>.

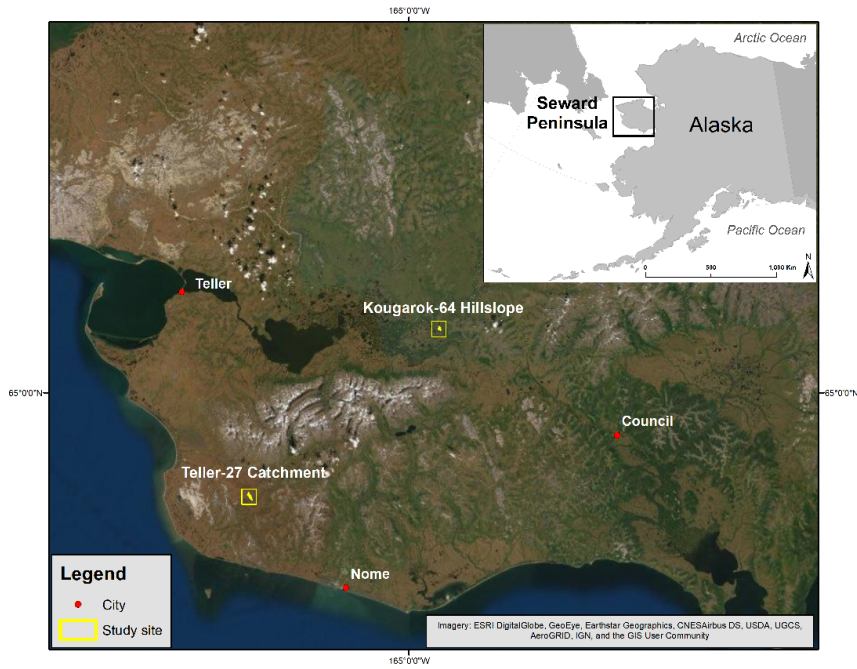
795 Wrona, F. J., Johansson, M., Culp, J. M., Jenkins, A., Mård, J., Myers-Smith, I. H., ... Wookey, P. A. 2016: Transitions  
796 in Arctic ecosystems: Ecological implications of a changing hydrological regime. *Journal of Geophysical Research:*  
797 *Biogeosciences*, 121: 650–674, doi: <https://doi.org/10.1002/2015JG003133>.

798 [Wulschleger, S. D., Epstein, H. E., Box, E. O., Euskirchen, E. S., Goswami, S., Iversen, C. M., et al. \(2014\). Plant](#)  
799 [functional types in earth system models: past experiences and future directions for application of dynamic vegetation](#)  
800 [models in high-latitude ecosystems. \*Ann. Bot.\* 114, 1–16. doi: 10.1093/aob/mcu077](#)

801 Yang, D., Meng, R., Morrison, B. D., McMahon, A., Hantson, W., Hayes, D. J., ... Serbin, S. P. 2020: A Multi-Sensor  
802 Unoccupied Aerial System Improves Characterization of Vegetation Composition and Canopy Properties in the Arctic  
803 Tundra. *Remote Sensing*, 12: 2638, doi: <https://doi.org/10.3390/rs12162638>.

804 [Yang, D., et al. "Landscape-Scale Characterization of Arctic Tundra Vegetation Composition, Structure, and Function](#)  
805 [with a Multi-Sensor Unoccupied Aerial System." \*Environmental Research Letters\* 16 \(8\), 085005 \(2021\).](#)  
806 <https://doi.org/10.1088/1748-9326/ac1291>.

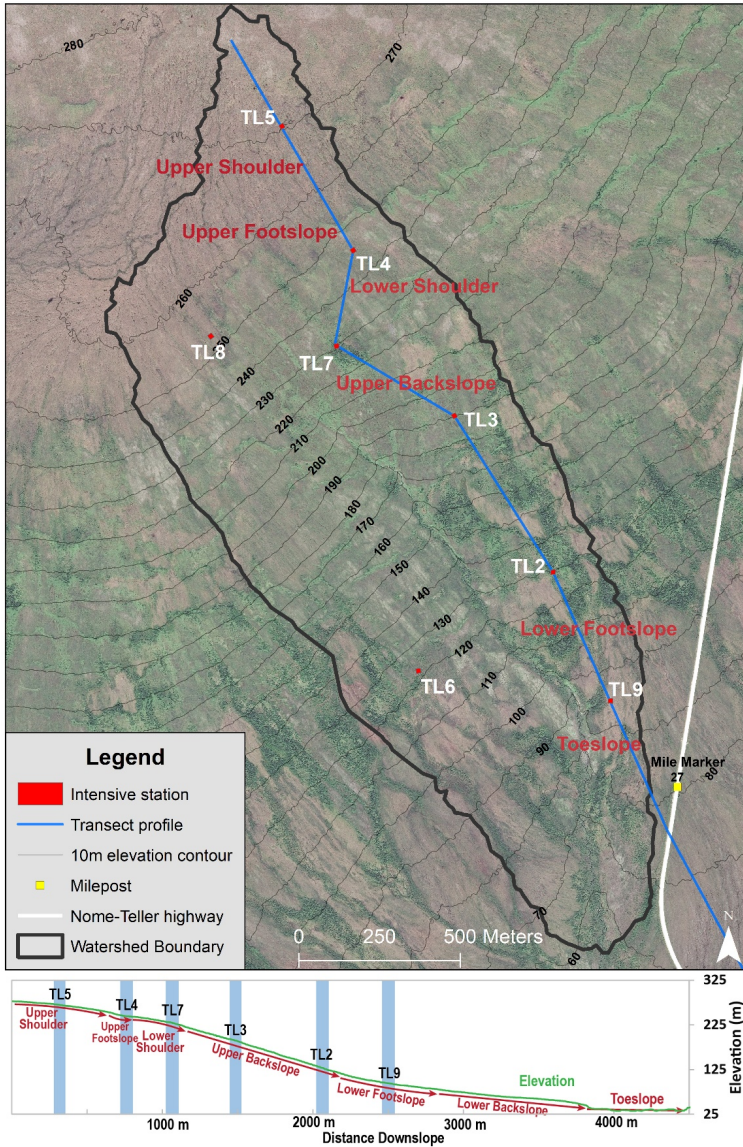
807



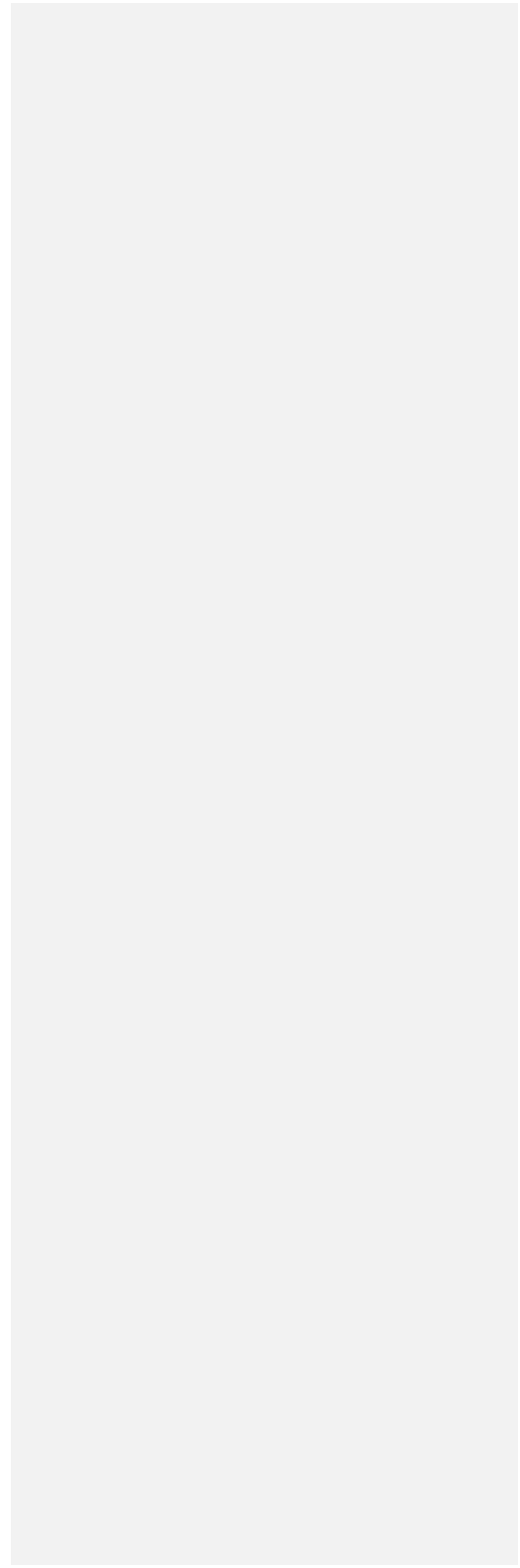
809  
810 **Figure 1. Location of the Teller and Kougarak field sites with respect to the municipalities of Teller, Nome, and Council.**  
811 **All are located on the Seward Peninsula in northwestern Alaska. RGB composite imagery from the 8-band WorldView-2**  
812 **imagery obtained on July 14, 2017 at 1.5 m resolution downloaded from the DigitalGlobe website**  
813 **(<https://www.digitalglobe.com/>).**

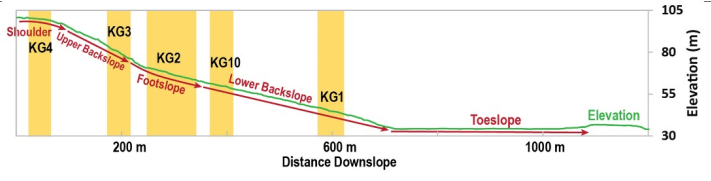
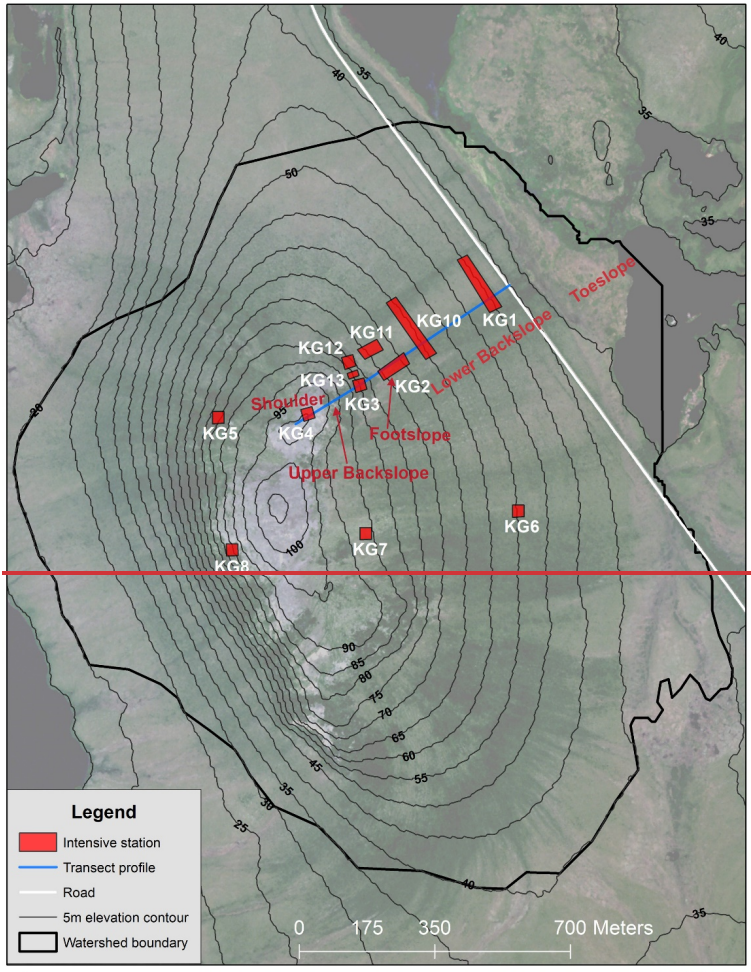
814  
815



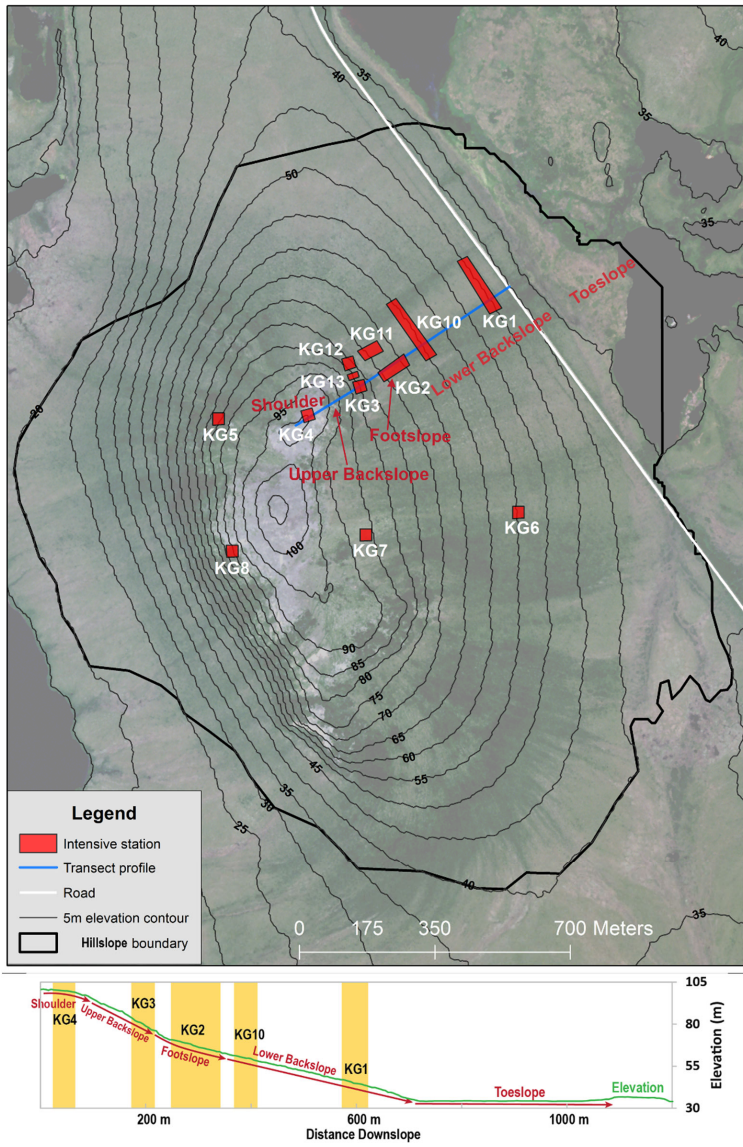


816  
 817 Figure 2. Topographic map of Teller. Station areas are shown as red polygons and the topographic station transect is given  
 818 as a solid blue line. The hillslope transect elevation profile is given below the map in green, with stations along the transect  
 819 in blue and hillslope positions noted with red arrows and text. RGB composite imagery from the 8-band WorldView-2  
 820 imagery obtained on July 27, 2011 at 1.5 m resolution downloaded from the DigitalGlobe website  
 821 (<https://www.digitalglobe.com/>).



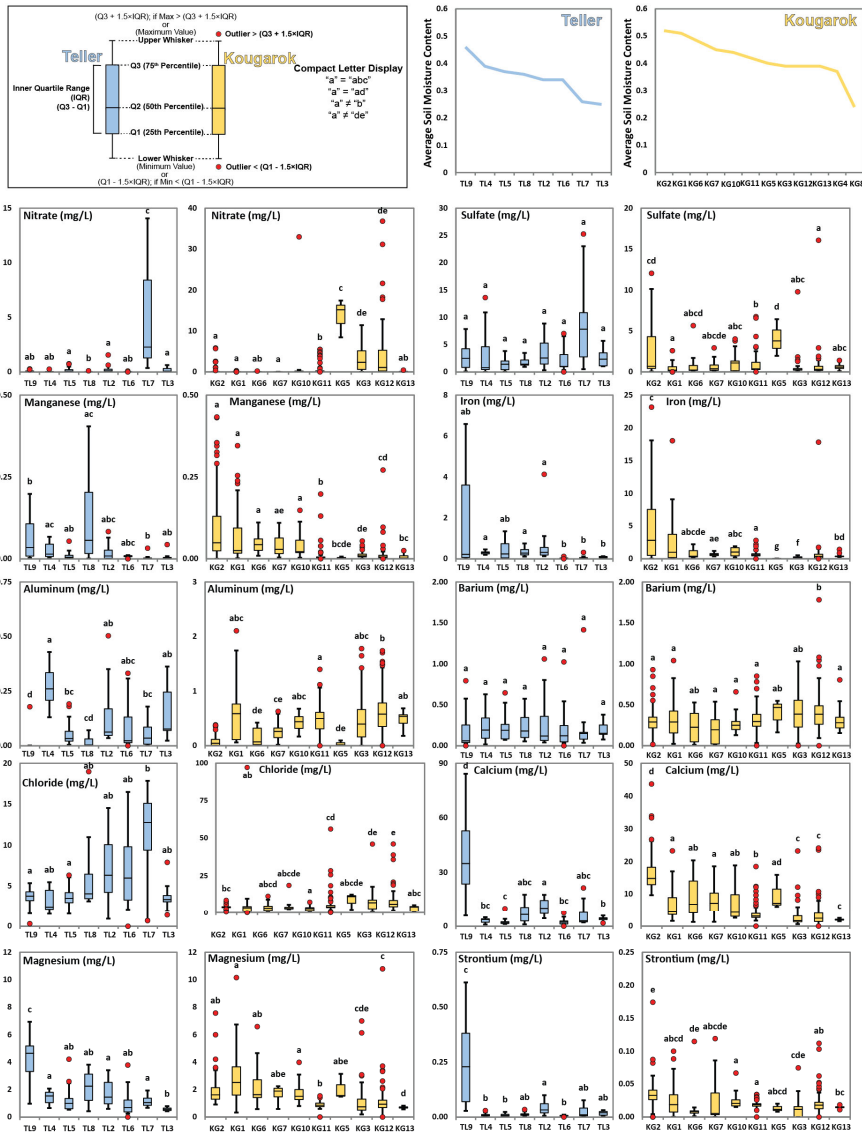


823

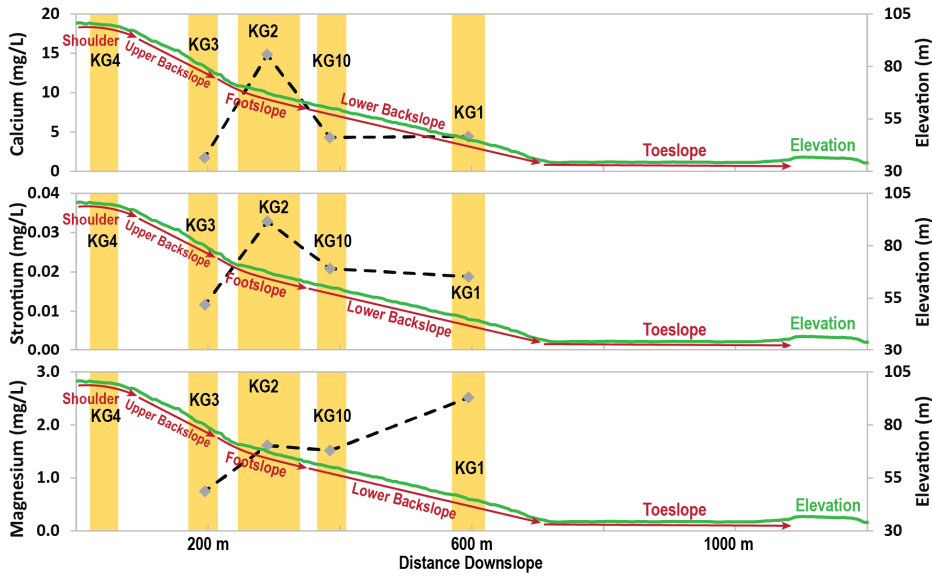
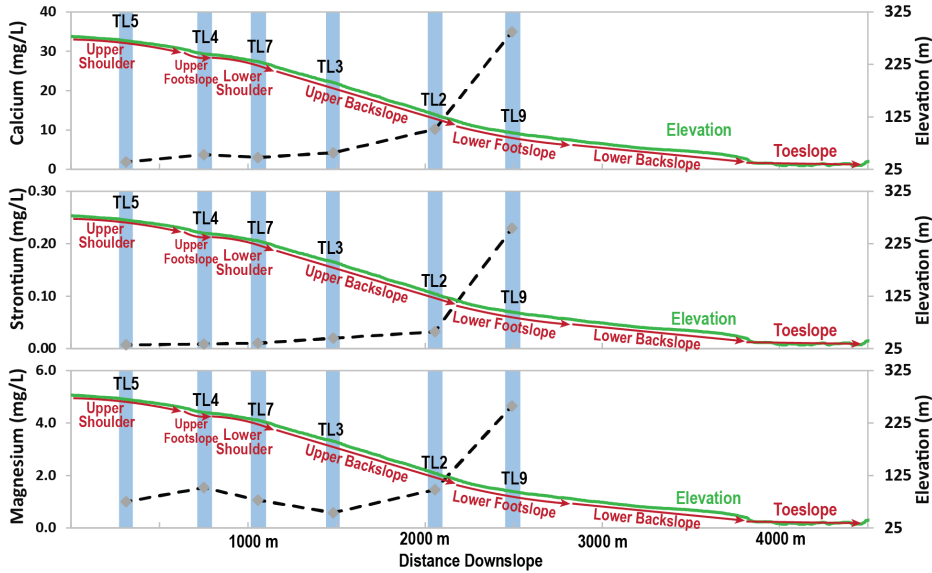


824

825 Figure 3. Topographic map of Kougarok. Station areas are shown as red polygons and the station transect is given as a  
 826 solid blue line. The transect elevation profile is given below the map in green, with stations along the transect in yellow and  
 827 hillslope positions noted with red arrows and text. RGB composite imagery from the 8-band WorldView-2 imagery obtained  
 828 on July 14, 2017 at 1.5 m resolution downloaded from the DigitalGlobe website (<https://www.digitalglobe.com/>).

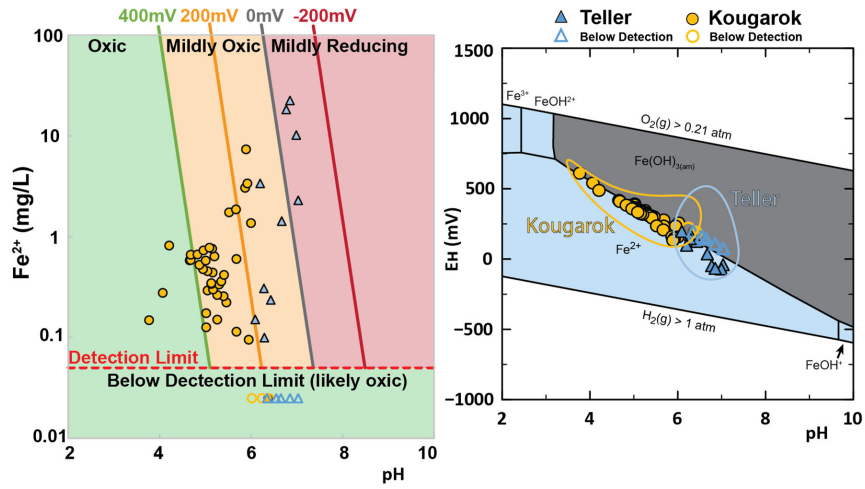


830  
 831 **Figure 4.** Mean COI concentrations at Teller (blue) and Kougarok (yellow) stations. Stations are arranged (left to right) by  
 832 soil moisture content determined by P-Band SAR (top right). Boxplots show the first, second, and third data quartiles, with  
 833 box whiskers representing either 150% of the inner quartile range (IQR), or the maximum or minimum value, when that  
 834 value was less than 1.5×IQR. Red circles represent data points outside of the 1.5×IQR whiskers (i.e. outliers). Note that the  
 835 concentration scales on the Teller and Kougarok plots often differ.



838 Figure 5. Median (50<sup>th</sup> percentile) concentrations (grey diamonds with dashed black lines) of Ca, Sr, and Mg, with distance  
 839 downslope at Teller (blue) and Kougarak (yellow) along topographic transects; areas of stations are indicated by blue and  
 840 yellow colouring, respectively. The elevation profiles of the hillslopes are plotted in green, on separate y-axes (right axes).  
 841 Topographic regions of both catchments are indicated by red arrows along the elevation gradient.

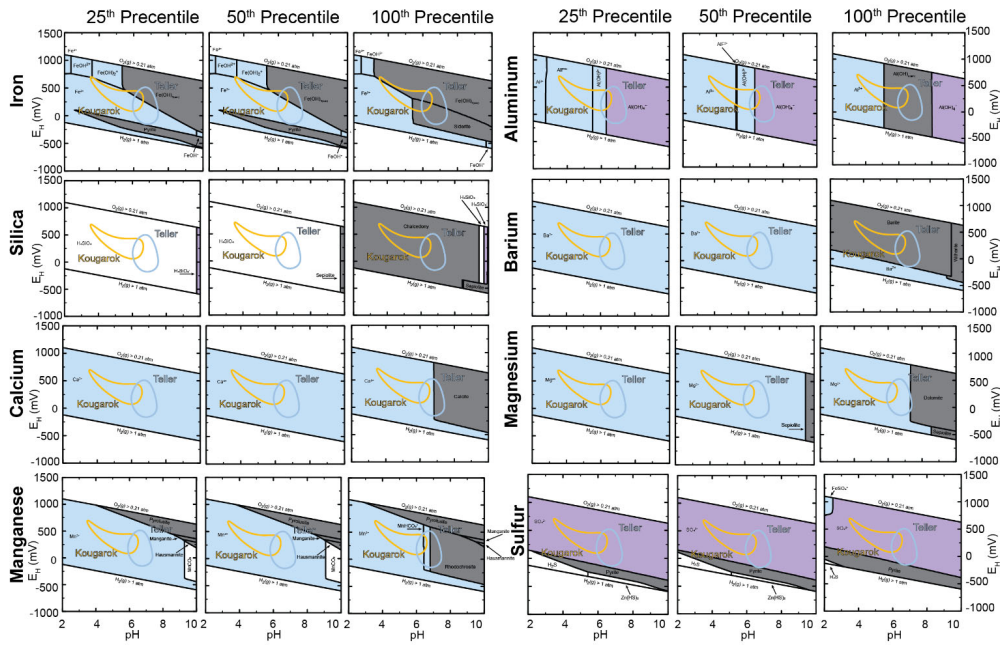
842



843

844 Figure 6. Left: Model-predicted Fe<sup>2+</sup> concentrations in saturated solutions of Fe(OH)<sub>3(am)</sub> at fixed E<sub>H</sub> conditions of 400 mV  
845 (green), 200 mV (orange), 0 mV (grey), and -200 mV (red), compared with field concentrations of Fe<sup>2+</sup> at Teller (red circles)  
846 and Kougarok (yellow circles). Right: Fe predominance diagram, showing the dominant specie of Fe under a range of  
847 Eh/pH conditions. Eh/pH regions relevant to Teller and Kougarok are outlined in blue and yellow, respectively. Samples  
848 with Fe<sup>2+</sup> concentrations below the detection limit are given as colour coordinated open circles set at 0.025 mg·L<sup>-1</sup> (half the  
849 detection limit) in both sides of the figure.

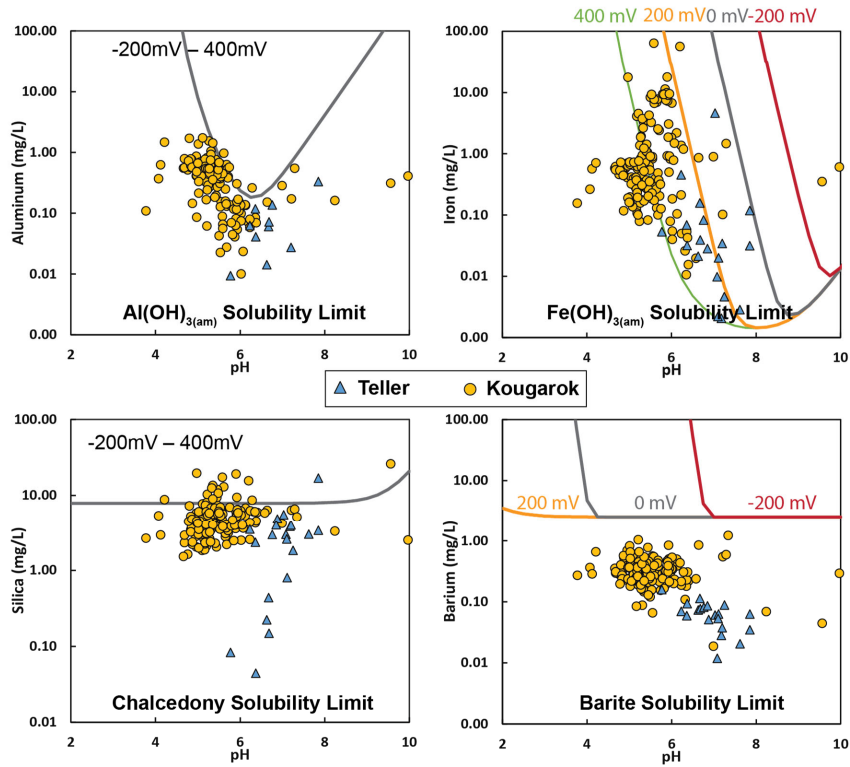
850



851  
 852 **Figure 7. Eh/pH diagrams for key species that indicated possible mineral formation under the Eh/pH conditions present at**  
 853 **either Teller or Kougarak. The Eh and pH conditions observed at Teller and Kougarak are overlaid as blue and yellow**  
 854 **lines, respectively. Mineral species (solids) are shown in grey, cations are shown in blue, anions are shown in purple,**  
 855 **neutral species are shown in white. Predominance diagrams were created in PhreePlot using the phreeqc.dat database, with**  
 856 **inorganic carbonate reduction to methane “turned off.”**



857



858

859 Figure 8. Modelled solute concentrations in solutions saturated with  $\text{Al(OH)}_{3(\text{am})}$ ,  $\text{Fe(OH)}_{3(\text{am})}$ , chalcedony, and barite, with  
860 respect to pH (x-axis) and  $E_{\text{H}}$  (model lines), overlaid with observed solute concentrations.

861

862 **910. Tables**

863 **Table 1. Teller Station Physical Characteristics**

	Hillslope Position	Vegetation				Relative wetness			Permafrost			
		Vegetation type	Average (maximum) canopy height (cm)	Dominant PFT	Low to tall shrub cover	Average TDR soil moisture (VMC)	Average P-band SAR (VMC)	Average snow depth (cm)	Average Ground Temperature (°C)	Permafrost Extent	Average (maximum) thaw depth (cm)	
TL9	Lower Foothslope		2834 (41)	Graminoid Bryophyte	44%	10%	NA	0.46	68.4	0	Marginal	101 (>20)
TL5	Upper Shoulder	Wetland complex	1234 (45)	Graminoid	45%	7%	0.55	0.37	103.3	-0.45	Near-surface	97' (>114')
TL8	Upper Foothslope		47 (34)	Bryophyte	33%	20%	0.55	0.36	77.7	-0.6		69' (>120)
TL3	Upper Backslope	Cassiope dwarf shrub	913 (23)	Evergreen dwarf shrub	47%	124%	NA	0.25	62.1	2.2	None/ deep	72' (82')
TL4	Upper Foothslope		40-8 (14)		58%	4%	0.35	0.39	89.5	0.5	Marginal	40' (70')
TL2	Upper Backslope	Mesic willow shrubland	8432 (141)	Deciduous low to tall shrub (willow)	44%	44%	0.4	0.34	124	2.4	None/ deep	75' (>120)
TL7	Lower Shoulder		468-151 (189)		37%	37%	0.46	0.26	128.8	2.4		51' (66')
TL6	Upper Backslope	Willow-birch tundra	74-64 (115)	ForbDeciduous-low shrub (willow & birch)	23%	32%	0.38	0.34	86.4	1.2	None/ deep	67' (102')

Formatted Table

864

865 PFT – plant functional type; dwarf shrub (height <40 cm), low shrub (height 40-200 cm), low to tall shrub (height 40 to >200 cm tall).  
 866 Deciduous shrub PFT classes identify the dominant species in the plant community as either willow or willow and birch. There is no alder at  
 867 the Teller site. Low to tall shrub cover represents the sum of deciduous low shrubs, deciduous low to potentially tall willow and birch, and  
 868 deciduous low to tall alder.

869 <sup>1</sup>Single point soil moisture measurements. Data are more accurate than P-band SAR but represent a much smaller spatial scale.

870 <sup>2</sup>P-band SAR has 30m resolution.

871 <sup>3</sup>Resistive layer was rock; all others are permafrost. A temperature probe was used to determine if the resistive layer was permafrost (≤0 °C)  
 872 or rock (>2 °C). Thaw depth is an average of 4 measurements from the vegetation plot corners within the IS and was measured at the end of  
 873 the growing season.  
 874

875 **Table 2. Kougarok Station Physical Characteristics**

	Hillslope Position	Vegetation				Relative wetness			Permafrost			
		Vegetation type	Average (maximum) canopy height (cm)	Dominant PFT		Low to tall shrub cover	Average TDR soil moisture (VMC)	Average P-band SAR (VMC)	Average snow depth (cm)	Average Ground Temperature (°C)	Permafrost Extent	Average (maximum) thaw depth (cm)
KG3	Upper Backslope	Alder shrubland	204 (265)	Deciduous low to tall shrub (alder)	30%	53% <sup>1</sup>	0.19	0.39	131.3	-0.01	Near-surface	48 <sup>2</sup> (53r)
KG12	Footslope		NA	NA	NA	NA	0.30*	0.39	NA	NA		NA <sup>3</sup>
KG1	Lower Backslope		60 (90)	Deciduous low shrub (alder, willow & birch)	31%	44% <sup>1</sup>	NA	0.51	83.4	-2.5		61 (68)
KG2	Footslope	Alder savanna in tussock tundra	48 (73)	Graminoid	30%	42% <sup>1</sup>	0.63	0.52	102.3	-1.2	Near-surface	75 (89)
KG6	Lower Backslope		24 (61)	Graminoid	46%	17% <sup>1</sup>	0.36	0.48	66.2	-2.2		58 (62)
KG10	Lower Backslope		NA	NA	NA	NA	NA*	0.44	71.4	NA		NA <sup>3</sup>
KG11	Footslope		NA	NA	NA	NA	0.59*	0.42	NA	NA		NA <sup>3</sup>
KG7	Upper Backslope	Tussock-lichen tundra	20 (22)	Graminoid	34%	14% <sup>1</sup>	0.51	0.45	54.7	-2.1	Near-surface	76 (100)
KG4	Shoulder	Dryas-lichen shrub tundra	6 (12)	Evergreen dwarf shrub	62%	1% <sup>1</sup>	NA	0.37	NA	-1.9	Near-surface	0 <sup>2</sup> (0 <sup>2</sup> )
KG13	Upper Backslope		NA	NA	NA	NA	0.41*	0.39	92.1	NA		NA <sup>3</sup>
KG5	Upper Backslope	Willow-birch tundra	62 (137)	Deciduous low shrub (willow & birch)	60%	62% <sup>1</sup>	NA	0.4	178.4	> 0	Deep	88 (96)
KG8	Upper Backslope		45 (120)	Evergreen dwarf shrub	52%	42% <sup>1</sup>	0.23	0.24	85.5	-0.04	Near-surface	44 <sup>2</sup> (58)

Formatted: Centered  
Formatted Table  
Formatted: Centered  
Formatted Table  
Formatted: Centered  
Formatted: Centered  
Formatted Table  
Formatted: Centered  
Formatted Table  
Formatted: Centered  
Formatted Table

876  
877  
878  
879  
880  
881  
882  
883  
884  
885

Note: PFT – plant functional type. Deciduous shrub PFT classes identify the dominant species in the community as either willow, alder, willow and birch, or alder, willow, and birch. Low to tall shrub cover represents the sum of deciduous low shrubs, deciduous low to potentially tall willow and birch, and deciduous low to tall alder.

<sup>1</sup>Single point soil moisture measurements. Data are more accurate than P-band SAR but represent a much smaller spatial scale.  
<sup>2</sup>P-band SAR has 30m resolution.  
\*Average gravimetric water content measurements, corrected to VMC by bulk density.  
<sup>3</sup>Resistive layer was rock; all others are permafrost. A temperature probe was used to determine if the resistive layer was permafrost ( $\leq 0$  °C) or rock ( $> 2$  °C). Thaw depth is an average of 4 measurements from the vegetation plot corners within the 1S and was measured at the end of the growing season.

Table 3. Inter-Site Mann-Whitney U-Test Results

	Teller			Kougarok			z	Site with Higher Median	Effect Size	Difference in Correlation
	n	Σ R <sub>i</sub>	U <sub>i</sub>	n	Σ R <sub>i</sub>	U <sub>i</sub>				
Na	59	3184	14811.5	275	52761.5	1413.5	9.95	Kougarok	0.54	large
F	59	3502	14375.5	273	51776.5	1731.5	9.46	Kougarok	0.52	large
K	59	3882	14113	275	52063	2112	8.92	Kougarok	0.49	medium-large
Si	59	4119	13876.5	275	51826.5	2348.5	8.56	Kougarok	0.47	medium-large
Al	58	4952	12709	275	50659	3241	7.11	Kougarok	0.39	medium
Oxalate	57	4996	12161.5	272	49289.5	3342.5	6.75	Kougarok	0.37	medium
B	59	5429	12566.5	275	50516.5	3658.5	6.62	Kougarok	0.36	medium
Zn	58	5605	12056	275	50006	3894	6.12	Kougarok	0.34	medium
SO <sub>4</sub>	58	13653	3892.5	273	41293.5	11941.5	6.08	Teller	0.33	medium
Fe	58	5958	11703	275	49653	4247	5.60	Kougarok	0.31	medium
Ba	58	6256	11405.5	275	49355.5	4544.5	5.15	Kougarok	0.28	medium
Ti	58	6266	11395.5	275	49345.5	4554.5	5.13	Kougarok	0.28	medium
NO <sub>2</sub>	54	5588	10585.5	272	47713.5	4102.5	5.12	Kougarok	0.28	medium
Li	58	7778	9883	275	47833	6067	2.86	Kougarok	0.16	small-medium
Br	58	8485	9060.5	273	46461.5	6773.5	1.73	Equal	0.09	small
NO <sub>3</sub>	58	8576	8969	273	46370	6865	1.59	Kougarok	0.09	small
Sr	58	8683	8978	275	46928	6972	1.51	Kougarok	0.08	small
PO <sub>4</sub>	54	9659	6460.5	271	43316.5	8173.5	1.36	Equal	0.08	small
Mg	58	10495	7166	275	45116	8784	1.21	Teller	0.07	small
Cr	58	8884	8777	275	46727	7173	1.20	Kougarok	0.07	small
Mn	58	9164	8497	275	46447	7453	0.78	Teller	0.04	small
Cl	58	9221	8266.5	272	45394.5	7509.5	0.57	Kougarok	0.03	small
Ca	58	10016	7645	275	45595	8305	0.50	Teller	0.03	small

Table 4. Dominant Environmental Controls on SPW Geochemistry at Teller and Kougarok

Environmental Control	Analytes Affected
Vegetation	<del>NO<sub>3</sub>NO<sub>2</sub><sup>-</sup></del>
Soil Moisture/Redox	<del>NO<sub>3</sub>NO<sub>2</sub><sup>-</sup></del> , Mn, Fe, SO <sub>4</sub> (occasionally)
Water/Soil Interactions & Hydrologic Transport	Ca, Mg, Sr
Mineral Solubility	Al, Ba, Si, Fe

Formatted: Subscript

Formatted: Subscript